Chapter 5

Multi-objective optimization of four recuperative gas turbine-based CCHP systems and 4E analyses at optimal conditions

This chapter presents four configurations of a gas turbine (GT)-based combined cooling heating and power (CCHP) systems. The proposed CCHP system configurations are retrofitted versions of combined power and cooling (CPC) systems which are already discussed in Chapter 3. The retrofitting is carried out with three major modifications as follows: replacing the simple GT cycle with a more efficient and cost-effective recuperative GT cycle as the prime mover, replacing the basic ORC with a more efficient and cost-effective recuperative-regenerative ORC (RR-ORC) and introducing water heat to produce hot water. Furthermore, the best optimal operating conditions are determined for the CCHP systems using multi-objective optimization technique. A comparative assessment of the four configurations of CCHP systems is also presented to choose the best-performing system.

5.1 Description of CCHP system configurations

The layout of proposed CCHP systems (system-I, system-II, system-III and system-IV) are shown in Figs. 5.1 to 5.4. The natural gas-fired recuperative GT cycle consists of an air compressor (AC), an air preheater (APH), a combustion chamber (CC), and a turbine. The hot combustion gases that exit the turbine are first utilized to heat the compressed air in the APH, and then to produce superheated steam in

the HRSG. The exhaust gas from the HRSG is then used to generate cooling in the absorption cooling system (ACS-II), and hot water is produced sequentially in the water heater (WH). The integrated GT-HRSG/ACS-II/WH setup is common in all four systems. The proposed systems differ in the manner in which the steam produced at the HRSG is used. The high-pressure steam expands in the back-pressure steam turbine (ST) in system-I (Fig. 5.1), and then 80% of the wet steam is extracted at an intermediate pressure for employing as a heat source to operate the RR-ORC. The rest 20% of the steam is expanded in the back-pressure ST to lower pressure and temperature which is suitable for operating another absorption cooling system (ACS-I). The two streams of steam supply the necessary heat for vapour generation in the RR-ORC's and ACS-I's generators, which are then pumped back to the HRSG after condensation.

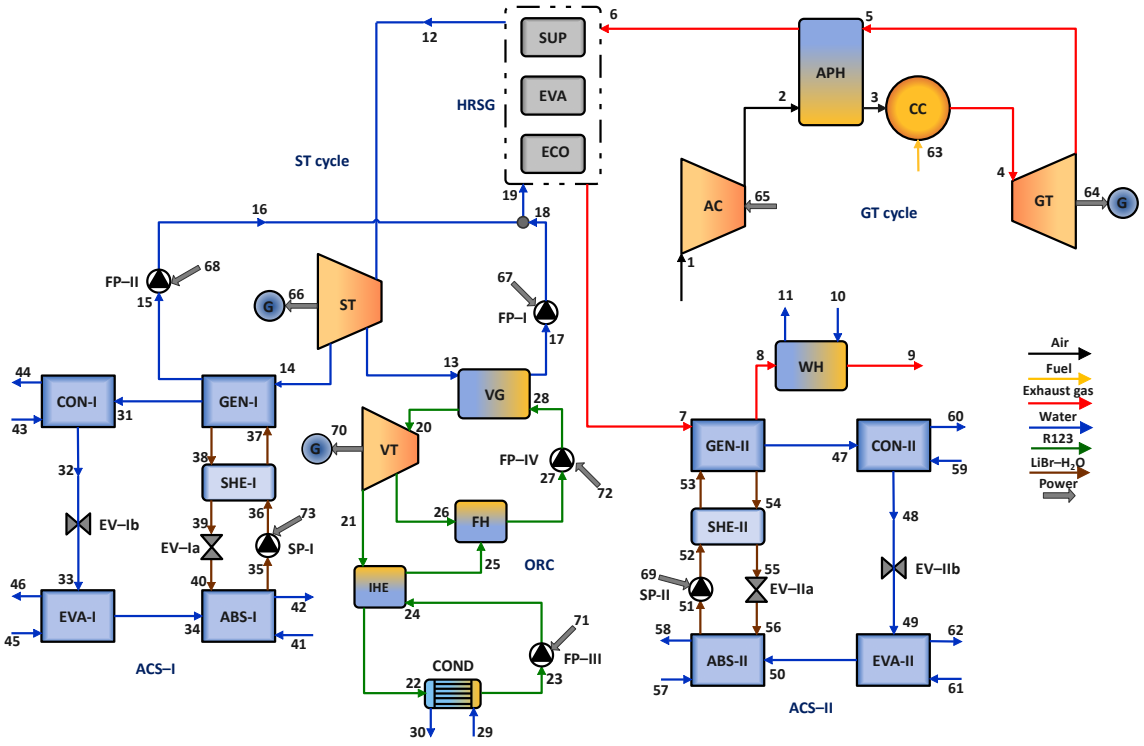

Fig. 5.1: Layout of the first CCHP system (CCHP system-I).

The layout of the second system (system-II) is shown in Fig. 5.2. It includes a back-pressure ST as well, where the steam expands to the necessary pressure before leaving. In contrast to system-I, which uses the steam from the back-pressure ST to run both the RR-ORC and the ACS-I, this system (system-II) only use the steam to run the RR-ORC. The wet steam from the back-pressure ST passes through the VG where it supplies heat for operating the RR-ORC. The phase of the steam changes from a wet condition to a liquid-saturated state while passing through the VG. The

water is then pumped to the HRSG for the next cycle. As already mentioned, the GT-HRSG/ACS-II/WH setup of the system-II is same as system-I.

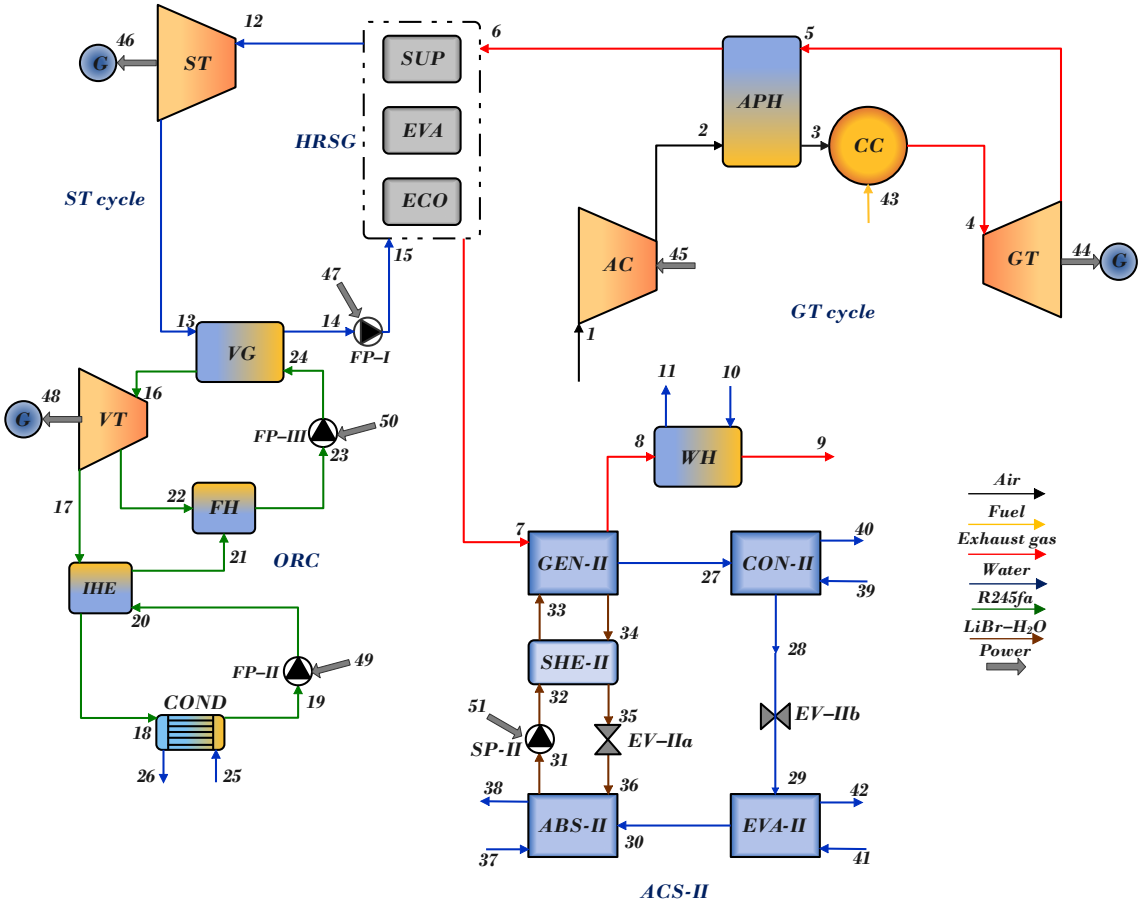

Fig. 5.2: Layout of the second CCHP system (CCHP system-II).

Further, the layout of the third system (system-III) is depicted in Fig. 5.3. In this system, a condensing ST cycle is used that includes a condenser and open water heater (OWH). The steam expands in the ST, and at a specific intermediate pressure, a fraction of the steam is withdrawn to pass through the OWH for feed water preheating. The remaining steam is expanded in the ST to the condenser pressure. The low-pressure steam then exits the ST and passes through the COND, where its phase changes to water. The condensed water from the condenser is then pumped back to the OWH where it is mixed with the extracted steam. The water from the exit of OWH is then pumped back to the HRSG for the next cycle.

The layout of the fourth system (system-IV) is shown in Fig. 5.4. In this system also, a condensing ST is used that includes a condenser and OWH. The steam expands in the ST, and at a certain intermediate pressure, 15% of the steam is extracted to pass it through the OWH for feed water preheating. The rest of the steam is expanded to a lower pressure at which 20% of the total steam is extracted for

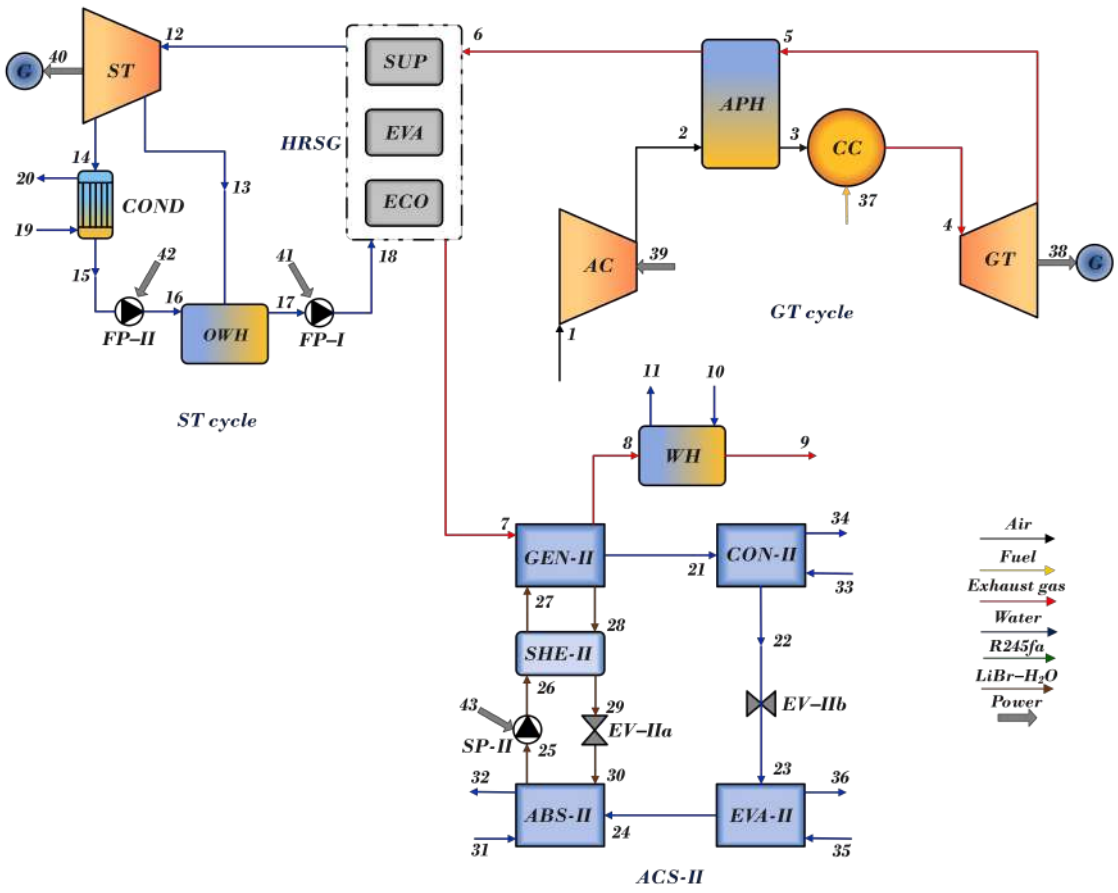

Fig. 5.3: Layout of the second CCHP system (CCHP system-III).

operating the ACS-I and the remaining steam is expanded to condenser pressure. The condensed water from the condenser and the generator of the ACS-I is then pumped back to the OWH and mixed with the extracted steam. The preheated water from the OWH is then pumped to the HRSG by using a feed pump.

5.2 Modelling

The assumptions and the input parameters considered for modelling the CCHP systems, and the mathematical formulations applied for performing the 4E analysis and the multi-objective optimization are discussed in the following subsections.

5.2.1 Assumptions

The general assumptions are given as follows [7, 25, 27, 33]:

- A relative humidity of 60%, a temperature of 298.15 K, and a pressure of 101.3 kPa are considered as ambient conditions.

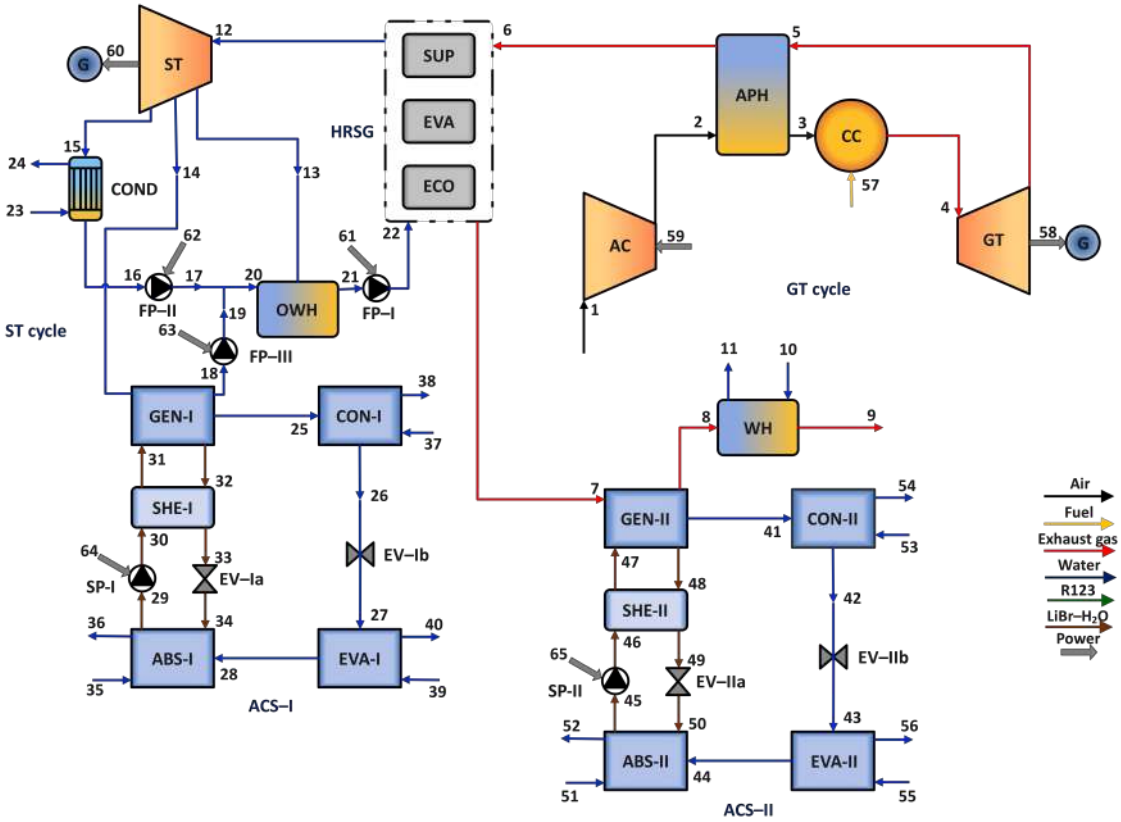

Fig. 5.4: Layout of the forth CCHP system (CCHP system-IV).

- The volumetric composition of fuel (natural gas) is:
  Methane (CH_4) 93.06%, Ethane (C_2H_6) 4.09%, Propane (C_3H_8) 0.99%, Butane (C_4H_{10}) 0.39%, Pentane (C_5H_{12}) 0.16%, Nitrogen (N_2) 0.4%, Carbon dioxide (CO_2) 0.89%.
- The heat exchanger's effectiveness is 75%.
- The chemical exergy of the working fluid in the RR-ORC is neglected.
- The pressure drop at the CC is assumed 3%.
- The pressure drop in the HRSG's gas side is 4%.
- The pressure drop in the VG and ACS's generators is 2%.
- Fuel pressure and temperature at the CC inlet are 2650 kPa and 333.35 K.

Tables 5.1 to 5.3 list the remaining parameters used in the modelling of the four CCHP system configurations.

Table 5.1: The parameters used in the modelling of the GT cycle [20, 26].

Parameters	Symbols	Value	Unit
Fuel flow rate	$\dot{m}_f$	2.56	kg/s
Air flow rate	$\dot{m}_a$	100	kg/s
AC pressure ratio	r_p	10	-
Isentropic efficiency of AC	$\eta_{s,AC}$	86	%
Isentropic efficiency of GT	$\eta_{s,GT}$	86	%
Combustion efficiency	η_{com}	98	%
Generator efficiency	η_{gen}	98	%
APH outlet temperature	T_3	810	K

Table 5.2: The parameters used in the modelling of the ST cycle and HRSG [26, 33].

Parameters	Symbols	Value	Unit
ST inlet pressure	P_{12}	8900	kPa
ST inlet temperature	T_{12}	823.15	K
ST isentropic efficiency	$\eta_{s,ST}$	90	%
FP isentropic efficiency	$\eta_{s,FP}$	90	%
COND pressure	P_{COND}	15	kPa
OWH pressure	P_{OWH}	200	kPa
HRSG's PPTD	$\Delta T_{pp,HRSG}$	30	K
HRSG's APTD	$\Delta T_{ap,HRSG}$	10	K

5.2.2 Energy analysis

The governing equations used to model the components of CCHP systems are the same as those used to model CPC systems (refer to Chapter 3). All of the components of CCHP systems are identical to those of CPC systems with the exception of three modifications: the inclusion of an air preheater or use of a recuperative GT cycle, the replacement of a recuperative ORC with an RR-ORC, and the addition of a water heater. Therefore, this subsection presents only the governing equations used to simulate the water heater and air preheaters. Further, the governing equations of RR-ORC are not discussed in the current chapter because the RR-ORC configuration has already been covered in Chapter 4.

Modelling of air preheater

The air preheater (APH) also known as a recuperator is a gas-to-gas direct heat exchanger which is primarily used in GTs to preheat compressed air by utilizing thermal energy from the turbine exhaust to improve energy efficiency. The recuperator facilitates heat exchange by directing the inlet air through a tube series and allowing the exhaust gas to pass over the same tubes. Notably, there is no mass

Table 5.3: The parameters used in the modelling of RR-ORC and ACS [25, 26, 30].

Parameters	Symbols	Value	Unit
VT inlet temperature (for system-I)	T_{20}	369	K
VT inlet temperature (for system-II)	T_{16}	375	K
COND temperature (for system-I)	T_{22}	303.15	K
COND temperature (for system-II)	T_{18}	303.15	K
Effectiveness of IHE	ω_{IHE}	90	%
Condensate inlet temperature (for system-I)	T_{29}	298.15	K
Condensate outlet temperature (for system-I)	T_{30}	303.15	K
Condensate inlet temperature (for system-II)	T_{25}	298.15	K
Condensate outlet temperature (for system-II)	T_{26}	303.15	K
VT isentropic efficiency	$\eta_{s,VT}$	90	%
VG's PPTD	$\Delta T_{pp,VG}$	10	K
FH pressure (for system-I)	P_{26}	384	kPa
FH pressure (for system-II)	P_{22}	384	kPa
ABS-I/II inlet water temperature	$T_{ABS-I/II,in}$	298.15	K
ABS-I/II outlet water temperature	$T_{ABS-I/II,out}$	303.15	K
EVA-I/II inlet water temperature	$T_{EVA-I/II,in}$	288.15	K
EVA-I/II outlet water temperature	$T_{EVA-I/II,out}$	283.15	K
CON-I/II inlet water temperature	$T_{CON-I/II,in}$	298.15	K
CON-I/II outlet water temperature	$T_{CON-I/II,out}$	303.15	K
GEN-I/II temperature	$T_{GEN-I/II}$	363.15	K
ABS-I/II temperature	$T_{ABS-I/II}$	308.15	K
CON-I/II temperature	$T_{CON-I/II}$	308.15	K
EVA-I/II temperature	$T_{EVA-I/II}$	278.15	K
SP-I/II isentropic efficiency	$\eta_{s,SP-I/II}$	90	%
SHE-I/II effectiveness	$\omega_{SHE-I/II}$	75	%

transfer between the two streams. The state points associated with the APH in four CCHP systems are the same. The properties of the compressed air at the inlet of the APH (state 2) are already obtained from the modelling of the AC. Similarly, the properties of the combustion gas at the inlet of the APH (state 5) are already obtained from the modelling of the GT. Meanwhile, the temperature of the compressed air at the outlet of the APH (state 3) is considered 810 K and the pressure is calculated by assuming a pressure drop of 3% [7]. Then using the temperature and pressure of state 3, the corresponding specific enthalpy and entropy are calculated using REFPROP 9.0 [22]. The temperature of the combustion gas at the outlet of the APH (state 6) is calculated using the heat balance equation given in Eq. (5.1) [7]. The pressure at state 6 is determined by assuming a pressure drop of 3%. Then again using the temperature and pressure of state 6, the corresponding

specific enthalpy and entropy are evaluated using REFPROP 9.0 [22].

$$h_6 = h_5 - \left(\frac{\dot{m}_a}{\dot{m}_g}\right)(h_3 - h_2) \tag{5.1}$$

Modelling of water heater

In the four CCHP systems, a shell and tube heat exchanger is used as water heaters to recover the heat from the flue gas to raise the temperature of water for various heating applications. The water heater does not change the state of the water and only performs sensible heating. In other words, the state of water at the inlet and outlet of the water heater is subcooled. The flue gas is passed through the tubes while the cold water is passed through the shell. The state properties of flue gas at the inlet of the water heater (state 9) are already known from the modelling of the ACS-II generator. The temperature of the flue gas at the outlet of the water heater is fixed at 373.15 K and the pressure is calculated considering a pressure drop of 3% [1]. The temperature of water at the inlet and outlet of the water heater is fixed at 298.15 K and 353.15 K [1]. The pressure of the water inlet to the water heater is considered 200 kPa without any pressure drop [1]. The specific enthalpy and entropy of all the state points associated with the water heater are evaluated by using REFPROP 9.0 [22]. Then the mass flow rate of hot water and process heat obtained from the water heater are determined by using Eq. (5.2) and Eq. (5.3), respectively.

$$\dot{m}_w = \dot{m}_g \left(\frac{h_8 - h_9}{h_{11} - h_{10}}\right) \tag{5.2}$$

$$\dot{Q}_{WH} = (h_{11} - h_{10}) \tag{5.3}$$

where $\dot{m}_w$ is the mass flow rate of hot water and $\dot{Q}_{WH}$ is process heat obtained from the water heater.

5.2.3 Exergy analysis

The physical and chemical exergy of each stream for all four CCHP systems is evaluated considering the same assumptions and correlations (Eqs. (3.22) to (3.30)) discussed in Chapter 3. Therefore, in this chapter those assumptions and correlations are not presented, rather the exergy balance equations formulated for each component of system-I to IV are displayed in Tables 5.4 to 5.7, respectively.

Table 5.4: Exergy balance equations for all components of system-I.

Components	System-I
AC	$\dot{E}_{65} = \dot{E}_2 - \dot{E}_1 + \dot{E}_D$
APH	$\dot{E}_5 - \dot{E}_6 = \dot{E}_3 - \dot{E}_2 + \dot{E}_D$
CC	$\dot{E}_3 + \dot{E}_{63} = \dot{E}_4 + \dot{E}_D$
GT	$\dot{E}_4 - \dot{E}_5 = \dot{E}_{64} + \dot{E}_{65} + \dot{E}_D$
HRSG	$\dot{E}_6 - \dot{E}_7 = \dot{E}_{12} - \dot{E}_{19} + \dot{E}_D$
ST	$\dot{E}_{12} - \dot{E}_{13} - \dot{E}_{14} = \dot{E}_{66} + \dot{E}_{67} + \dot{E}_{68} + \dot{E}_{69} + \dot{E}_D$
VG	$\dot{E}_{13} - \dot{E}_{17} = \dot{E}_{20} - \dot{E}_{28} + \dot{E}_D$
VT	$\dot{E}_{20} - \dot{E}_{21} - \dot{E}_{26} = \dot{E}_{70} + \dot{E}_{71} + \dot{E}_{72} + \dot{E}_{73} + \dot{E}_D$
IHE	$\dot{E}_{21} - \dot{E}_{22} = \dot{E}_{25} - \dot{E}_{24} + \dot{E}_D$
COND	$\dot{E}_{22} - \dot{E}_{23} = \dot{E}_{30} - \dot{E}_{29} + \dot{E}_D$
FH	$\dot{E}_{22} - \dot{E}_{23} = \dot{E}_{30} - \dot{E}_{29} + \dot{E}_D$
FP-I	$\dot{E}_{67} = \dot{E}_{18} - \dot{E}_{17} + \dot{E}_D$
FP-II	$\dot{E}_{68} = \dot{E}_{16} - \dot{E}_{15} + \dot{E}_D$
FP-III	$\dot{E}_{71} = \dot{E}_{24} - \dot{E}_{23} + \dot{E}_D$
FP-IV	$\dot{E}_{72} = \dot{E}_{28} - \dot{E}_{27} + \dot{E}_D$
GEN-I	$\dot{E}_7 - \dot{E}_8 = \dot{E}_{47} + \dot{E}_{54} - \dot{E}_{53} + \dot{E}_D$
ABS-I	$\dot{E}_{26} + \dot{E}_{32} - \dot{E}_{27} = \dot{E}_{34} - \dot{E}_{33} + \dot{E}_D$
CON-I	$\dot{E}_{23} - \dot{E}_{24} = \dot{E}_{36} - \dot{E}_{35} + \dot{E}_D$
EVA-I	$\dot{E}_{25} - \dot{E}_{26} = \dot{E}_{38} - \dot{E}_{37} + \dot{E}_D$
SHE-I	$\dot{E}_{30} - \dot{E}_{31} = \dot{E}_{29} - \dot{E}_{28} + \dot{E}_D$
SP-I	$\dot{E}_{61} = \dot{E}_{28} - \dot{E}_{27} + \dot{E}_D$
GEN-II	$\dot{E}_7 - \dot{E}_8 = \dot{E}_{47} + \dot{E}_{54} - \dot{E}_{53} + \dot{E}_D$
ABS-II	$\dot{E}_{56} + \dot{E}_{50} - \dot{E}_{58} = \dot{E}_{57} - \dot{E}_{49} + \dot{E}_D$
CON-II	$\dot{E}_{47} - \dot{E}_{48} = \dot{E}_{60} - \dot{E}_{59} + \dot{E}_D$
EVA-II	$\dot{E}_{49} - \dot{E}_{50} = \dot{E}_{62} - \dot{E}_{61} + \dot{E}_D$
SHE-II	$\dot{E}_{54} - \dot{E}_{55} = \dot{E}_{53} - \dot{E}_{52} + \dot{E}_D$
SP-II	$\dot{E}_{69} = \dot{E}_{52} - \dot{E}_{51} + \dot{E}_D$
WH	$\dot{E}_8 - \dot{E}_9 = \dot{E}_{11} - \dot{E}_{10} + \dot{E}_D$

5.2.4 Exergoeconomic analysis

The exergoeconomic analysis of all four CCHP systems is performed considering the same assumptions and correlations (Eqs. (4.4) to (4.15)) discussed in Chapter 4. Therefore, in this chapter those assumptions and correlations are not presented, rather the cost balance equations formulated for each component of system-I to IV are displayed in Tables 5.8 to 5.11, respectively. The mathematical functions used for evaluating the purchase equipment cost of all the equipment of the CCHP systems are evaluated by applying Eqs. (5.4) to (5.20). However, the mathematical functions used for the evaluation of purchase equipment costs of RR-ORC components are not presented in this chapter because those were already provided in Chapter 4

Table 5.5: Exergy balance equations for all components of system-II.

Components	System-II
AC	$\dot{E}_{45} = \dot{E}_2 - \dot{E}_1 + \dot{E}_D$
APH	$\dot{E}_5 - \dot{E}_6 = \dot{E}_3 - \dot{E}_2 + \dot{E}_D$
CC	$\dot{E}_3 + \dot{E}_{43} = \dot{E}_4 + \dot{E}_D$
GT	$\dot{E}_4 - \dot{E}_5 = \dot{E}_{44} + \dot{E}_{45} + \dot{E}_D$
HRSG	$\dot{E}_6 - \dot{E}_7 = \dot{E}_{12} - \dot{E}_{15} + \dot{E}_D$
ST	$\dot{E}_{12} - \dot{E}_{13} = \dot{E}_{46} + \dot{E}_{47} + \dot{E}_D$
VG	$\dot{E}_{13} - \dot{E}_{14} = \dot{E}_{16} - \dot{E}_{24} + \dot{E}_D$
VT	$\dot{E}_{16} - \dot{E}_{17} - \dot{E}_{22} = \dot{E}_{48} + \dot{E}_{49} + \dot{E}_{50} + \dot{E}_{51} + \dot{E}_D$
IHE	$\dot{E}_{17} - \dot{E}_{18} = \dot{E}_{21} - \dot{E}_{20} + \dot{E}_D$
COND	$\dot{E}_{18} - \dot{E}_{19} = \dot{E}_{26} - \dot{E}_{25} + \dot{E}_D$
FH	$\dot{E}_{18} - \dot{E}_{19} = \dot{E}_{26} - \dot{E}_{25} + \dot{E}_D$
FP-I	$\dot{E}_{47} = \dot{E}_{15} - \dot{E}_{14} + \dot{E}_D$
FP-II	$\dot{E}_{49} = \dot{E}_{20} - \dot{E}_{19} + \dot{E}_D$
FP-III	$\dot{E}_{50} = \dot{E}_{24} - \dot{E}_{23} + \dot{E}_D$
GEN-II	$\dot{E}_7 - \dot{E}_8 = \dot{E}_{27} + \dot{E}_{34} - \dot{E}_{33} + \dot{E}_D$
ABS-II	$\dot{E}_{30} + \dot{E}_{36} - \dot{E}_{31} = \dot{E}_{38} - \dot{E}_{37} + \dot{E}_D$
CON-II	$\dot{E}_{27} - \dot{E}_{28} = \dot{E}_{40} - \dot{E}_{39} + \dot{E}_D$
EVA-II	$\dot{E}_{29} - \dot{E}_{30} = \dot{E}_{42} - \dot{E}_{41} + \dot{E}_D$
SHE-II	$\dot{E}_{34} - \dot{E}_{35} = \dot{E}_{33} - \dot{E}_{32} + \dot{E}_D$
SP-II	$\dot{E}_{51} = \dot{E}_{32} - \dot{E}_{31} + \dot{E}_D$
WH	$\dot{E}_8 - \dot{E}_9 = \dot{E}_{11} - \dot{E}_{10} + \dot{E}_D$

Table 5.6: Exergy balance equations for all components of system-III.

Components	System-II
AC	$\dot{E}_{39} = \dot{E}_2 - \dot{E}_1 + \dot{E}_D$
APH	$\dot{E}_5 - \dot{E}_6 = \dot{E}_3 - \dot{E}_2 + \dot{E}_D$
CC	$\dot{E}_3 + \dot{E}_{37} = \dot{E}_4 + \dot{E}_D$
GT	$\dot{E}_4 - \dot{E}_5 = \dot{E}_{38} + \dot{E}_{39} + \dot{E}_D$
HRSG	$\dot{E}_6 - \dot{E}_7 = \dot{E}_{12} - \dot{E}_{18} + \dot{E}_D$
ST	$\dot{E}_{12} - \dot{E}_{13} - \dot{E}_{14} = \dot{E}_{40} + \dot{E}_{41} + \dot{E}_{42} + \dot{E}_{43} + \dot{E}_D$
OWH	$\dot{E}_{13} + \dot{E}_{16} = \dot{E}_{17} + \dot{E}_D$
COND	$\dot{E}_{14} - \dot{E}_{15} = \dot{E}_{20} - \dot{E}_{19} + \dot{E}_D$
FP-I	$\dot{E}_{41} = \dot{E}_{18} - \dot{E}_{17} + \dot{E}_D$
FP-II	$\dot{E}_{42} = \dot{E}_{16} - \dot{E}_{15} + \dot{E}_D$
GEN-II	$\dot{E}_7 - \dot{E}_8 = \dot{E}_{21} + \dot{E}_{28} - \dot{E}_{27} + \dot{E}_D$
ABS-II	$\dot{E}_{30} + \dot{E}_{24} - \dot{E}_{25} = \dot{E}_{32} - \dot{E}_{31} + \dot{E}_D$
CON-II	$\dot{E}_{21} - \dot{E}_{22} = \dot{E}_{34} - \dot{E}_{33} + \dot{E}_D$
EVA-II	$\dot{E}_{23} - \dot{E}_{24} = \dot{E}_{36} - \dot{E}_{35} + \dot{E}_D$
SHE-II	$\dot{E}_{28} - \dot{E}_{29} = \dot{E}_{33} - \dot{E}_{32} + \dot{E}_D$
SP-II	$\dot{E}_{43} = \dot{E}_{27} - \dot{E}_{26} + \dot{E}_D$
WH	$\dot{E}_8 - \dot{E}_9 = \dot{E}_{11} - \dot{E}_{10} + \dot{E}_D$

Table 5.7: Exergy balance equations for all components of system-IV.

Components	System-IV
AC	$\dot{E}_{59} = \dot{E}_2 - \dot{E}_1 + \dot{E}_D$
APH	$\dot{E}_5 - \dot{E}_6 = \dot{E}_3 - \dot{E}_2 + \dot{E}_D$
CC	$\dot{E}_3 + \dot{E}_{57} = \dot{E}_4 + \dot{E}_D$
GT	$\dot{E}_4 - \dot{E}_5 = \dot{E}_{58} + \dot{E}_{59} + \dot{E}_D$
HRSG	$\dot{E}_6 - \dot{E}_7 = \dot{E}_{12} - \dot{E}_{22} + \dot{E}_D$
ST	$\dot{E}_{12} - \dot{E}_{13} - \dot{E}_{14} - \dot{E}_{15} = \dot{E}_{60} + \dot{E}_{61} + \dot{E}_{62} + \dot{E}_{63} + \dot{E}_{64} + \dot{E}_{65} + \dot{E}_D$
OWH	$\dot{E}_{13} + \dot{E}_{20} = \dot{E}_{21} + \dot{E}_D$
COND	$\dot{E}_{15} - \dot{E}_{16} = \dot{E}_{24} - \dot{E}_{23} + \dot{E}_D$
FP-I	$\dot{E}_{61} = \dot{E}_{22} - \dot{E}_{21} + \dot{E}_D$
FP-II	$\dot{E}_{62} = \dot{E}_{17} - \dot{E}_{16} + \dot{E}_D$
FP-III	$\dot{E}_{63} = \dot{E}_{19} - \dot{E}_{18} + \dot{E}_D$
GEN-I	$\dot{E}_{14} - \dot{E}_{18} = \dot{E}_{25} + \dot{E}_{32} - \dot{E}_{31} + \dot{E}_D$
ABS-I	$\dot{E}_{34} + \dot{E}_{28} - \dot{E}_{29} = \dot{E}_{36} - \dot{E}_{35} + \dot{E}_D$
CON-I	$\dot{E}_{25} - \dot{E}_{26} = \dot{E}_{38} - \dot{E}_{37} + \dot{E}_D$
EVA-I	$\dot{E}_{27} - \dot{E}_{28} = \dot{E}_{40} - \dot{E}_{39} + \dot{E}_D$
SHE-I	$\dot{E}_{32} - \dot{E}_{33} = \dot{E}_{31} - \dot{E}_{30} + \dot{E}_D$
SP-I	$\dot{E}_{64} = \dot{E}_{30} - \dot{E}_{29} + \dot{E}_D$
GEN-II	$\dot{E}_7 - \dot{E}_8 = \dot{E}_{41} + \dot{E}_{48} - \dot{E}_{47} + \dot{E}_D$
ABS-II	$\dot{E}_{44} + \dot{E}_{50} - \dot{E}_{45} = \dot{E}_{52} - \dot{E}_{51} + \dot{E}_D$
CON-II	$\dot{E}_{41} - \dot{E}_{42} = \dot{E}_{54} - \dot{E}_{55} + \dot{E}_D$
EVA-II	$\dot{E}_{43} - \dot{E}_{44} = \dot{E}_{56} - \dot{E}_{55} + \dot{E}_D$
SHE-II	$\dot{E}_{48} - \dot{E}_{49} = \dot{E}_{47} - \dot{E}_{46} + \dot{E}_D$
SP-II	$\dot{E}_{65} = \dot{E}_{46} - \dot{E}_{45} + \dot{E}_D$
WH	$\dot{E}_8 - \dot{E}_9 = \dot{E}_{11} - \dot{E}_{10} + \dot{E}_D$

(Table 4.5). Moreover, the purchase equipment costs are updated from the original year to the reference year (2022) by using Eq. (4.9) [6]. Meanwhile, the heat transfer areas of the WH and the COND are calculated by assuming those as shell and tube heat exchangers. The methodology for modelling the shell and tube heat exchangers reported in Ref. [34] is implemented in this study.

AC: The cost function to evaluate the purchase equipment cost of the air compressor is given as follows [7]:

$$PEC_{AC} = \left(\frac{71.10\dot{m}_a}{0.90 - \eta_{s,AC}}\right)\left(\frac{P_2}{P_1}\right) ln\left(\frac{P_2}{P_1}\right) \tag{5.4}$$

where PEC_{AC} is based on 1995 with the cost index of 1020.4 [7, 20] and $\dot{m}_a$ is the mass flow rate of air, $\eta_{s,AC}$ is the isentropic efficiency of AC, P_1 is the air compressor inlet pressure and P_2 is the AC outlet pressure.

APH: The cost function to evaluate the purchase equipment cost of the APH is

given as follows [7]:

$$PEC_{APH} = \left[4122\left(\frac{\dot{m}_g(h_5 - h_6)}{18 \times \Delta T_{lm,APH}}\right)\right]^{0.6} \tag{5.5}$$

where PEC_{APH} is based on 1995 with the cost index of 1020.4 [7, 20], $\dot{m}_g$ is the mass flow rate of flue gas and $\Delta T_{lm,APH}$ is the log mean temperature difference of the APH.

CC: The cost function to evaluate the purchase equipment cost of the CC is given as follows [7]:

$$PEC_{CC} = \frac{46.08\dot{m}_a}{[0.995 - P_4/P_3]}[1 + exp(0.018T_4 - 26.4)] \tag{5.6}$$

where PEC_{CC} is based on 1995 with the cost index of 1020.4 [7, 20] and T_4 is the flue gas temperature at the CC outlet, P_3 is the air temperature at the CC inlet and P_4 is the flue gas temperature at the CC outlet.

GT: The cost function to evaluate the purchase equipment cost of the GT is given as follows [7]:

$$PEC_{GT} = \left(\frac{479.34\dot{m}_g}{0.92 - \eta_{s,GT}}\right) ln\left(\frac{P_4}{P_5}\right)[1 + exp(0.036T_4 - 54.4)] \tag{5.7}$$

where PEC_{GT} is based on 1995 with the cost index of 1020.4 [7, 20], $\eta_{s,GT}$ is the isentropic efficiency of GT and P_5 is the GT outlet pressure.

ST: The cost function to evaluate the purchase equipment cost of the ST is given as follows [13]:

$$PEC_{ST} = 3880.5 \times \dot{W}_{ST}^{0.7}\left(1 + \left(\frac{0.05}{1 - \eta_{s,ST}}\right)^3\right) \times \left(1 + 5 \times exp\left(\frac{T_{12} - 866}{10.42}\right)\right) \tag{5.8}$$

where PEC_{ST} is based on 2003 with the cost index of 1113.1 [13, 20] and $\eta_{s,ST}$ is the isentropic efficiency of ST, T_{12} is the ST inlet temperature and $\dot{W}_{ST}$ is the power output of the ST.

HRSG: The cost function to evaluate the purchase equipment cost of the HRSG is given as follows [7]:

$$PEC_{HRSG} = 6570\sum_k\left(\frac{\dot{Q}_k}{\Delta T_{lm,k}}\right)^{0.8} + 21276\dot{m}_s + 1184.4\dot{m}_g^{1.2} \tag{5.9}$$

where PEC_{HRSG} is based on 1995 with the cost index of 1020.4 [7, 20], $\dot{m}_s$ is the

mass flow rate of steam, $\dot{Q}_k$ and $\Delta T_{lm,k}$ are the heat transfer rate and the log mean temperature difference of economizer, evaporator and superheater, respectively.

COND: The cost function to evaluate the purchase equipment cost of the COND employed in the ST cycle is given as follows [24]:

$$PEC_{COND} = 588 \times A^{0.8} \tag{5.10}$$

where PEC_{COND} is based on 2005 with the cost index of 1218.0 [20, 24] and A is the heat transfer rate of the COND.

OWH: The cost function to evaluate the purchase equipment cost of the OWH employed in the ST cycle is given as follows [6]:

$$PEC_{OWH} = (527.7/397)^{1.7} \times \acute{C} \tag{5.11}$$

where

$$\log_{10} \acute{C} = 4.20 - 0.204 \log_{10} \dot{V} + 0.1245(\log_{10} \dot{V})^2 \tag{5.12}$$

where PEC_{OWH} is based on 2013 with the cost index of 1552.8 [6, 20] and $\dot{V}$ is the volume flow rate of turbine bleed.

FPs: The cost function to evaluate the purchase equipment cost of FPs is given as follows [6]:

$$PEC_{FP} = 3540(\dot{W}_{FP}^{0.71}) \tag{5.13}$$

where PEC_{FP} is based on 2011 with the cost index of 1476.7 [6, 20] and $\dot{W}_{FP}$ is the power consumed by the FP.

GEN: The cost function to evaluate the purchase equipment cost of GEN (GEN-I and GEN-II) is given as follows [35]:

$$PEC_{GEN} = PEC_{ref,GEN} \left(\frac{A_{GEN}}{A_{ref,GEN}} \right)^{0.6} \tag{5.14}$$

where PEC_{GEN} is based on 2000 with the cost index of 1069.6 [20, 35], $A_{ref} = 100\ m^2$ and $PEC_{ref,GEN}$=17500 $ [35].

EVA: The cost function to evaluate the purchase equipment cost of EVA (EVA-I and EVA-II) is given as follows [35]:

$$PEC_{EVA} = PEC_{ref,EVA} \left(\frac{A_{EVA}}{A_{ref,EVA}} \right)^{0.6} \tag{5.15}$$

where PEC_{EVA} is based on 2000 with the cost index of 1069.6 [20, 35], $A_{ref} =$

100 m^2 and $PEC_{ref,EVA}$=16000 $ [35].

ABS: The cost function to evaluate the purchase equipment cost of ABS (ABS-I and ABS-II) is given as follows [35]:

$$PEC_{ABS} = PEC_{ref,ABS} \left(\frac{A_{ABS}}{A_{ref,ABS}} \right)^{0.6} \tag{5.16}$$

where PEC_{ABS} is based on 2000 with the cost index of 1069.6 [20, 35], $A_{ref} = 100\ m^2$ and $PEC_{ref,ABS}$=16500 $ [35].

CON: The cost function to evaluate the purchase equipment cost of CON (CON-I and CON-II) is given as follows [35]:

$$PEC_{CON} = PEC_{ref,CON} \left(\frac{A_{CON}}{A_{ref,CON}} \right)^{0.6} \tag{5.17}$$

where PEC_{CON} is based on 2000 with the cost index of 1069.6 [20, 35], $A_{ref} = 100\ m^2$ and $PEC_{ref,CON}$=8000 $ [35].

SHE: The cost function to evaluate the purchase equipment cost of SHE (SHE-I and SHE-II) is given as follows [35]:

$$PEC_{SHE} = PEC_{ref,SHE} \left(\frac{A_{SHE}}{A_{ref,SHE}} \right)^{0.6} \tag{5.18}$$

where PEC_{SHE} is based on 2000 with the cost index of 1069.6 [20, 35], $A_{ref} = 100\ m^2$ and $PEC_{ref,SHE}$=12000 $ [35].

SP: The cost function to evaluate the purchase equipment cost of SP is given as follows [6]:

$$PEC_{SP} = 3540(\dot{W}_{SP}^{0.71}) \tag{5.19}$$

where PEC_{SP} is based on 2011 with the cost index of 1476.7 [6, 20] and $\dot{W}_{SP}$ is the power consumed by the SP.

WH: The cost function to evaluate the purchase equipment cost of the WH is given as follows [10]:

$$PEC_{WH} = 130 \times \left(\frac{A}{0.093} \right)^{0.78} \tag{5.20}$$

where PEC_{WH} is based on 2005 with the cost index of 1218.0 [10, 20] and A is the heat transfer rate of the WH.

Table 5.8: Cost balance equations for each component of the system–I.

Components	Cost balance equations
AC	$\dot{C}_1 + \dot{C}_{65} + \dot{Z}_{AC} = \dot{C}_2$
	$\dot{C}_1 = 0$
APH	$\dot{C}_2 + \dot{C}_5 + \dot{Z}_{APH} = \dot{C}_3 + \dot{C}_6$
	$c_5 = c_6$
CC	$\dot{C}_3 + \dot{C}_{63} + \dot{Z}_{CC} = \dot{C}_4$
	$\dot{C}_{63} = c_f \dot{m}_f LHV$
GT	$\dot{C}_4 + \dot{Z}_{GT} = \dot{C}_5 + \dot{C}_{64} + \dot{C}_{65}$
	$c_4 = c_5$, $c_{64} = c_{65}$
HRSG	$\dot{C}_6 + \dot{C}_{19} + \dot{Z}_{HRSG} = \dot{C}_7 + \dot{C}_{12}$
	$c_6 = c_7$
	$\dot{C}_{11} + \dot{C}_{13} = \dot{C}_{14}$
ST	$\dot{C}_{12} + \dot{Z}_{ST} = \dot{C}_{13} + \dot{C}_{14} + \dot{C}_{66} + \dot{C}_{67} + \dot{C}_{68} + \dot{C}_{69}$
	$c_{12} = c_{13}$, $c_{12} = c_{14}$, $c_{66} = c_{67}$, $c_{66} = c_{68}$, $c_{66} = c_{69}$
VG	$\dot{C}_{13} + \dot{C}_{28} + \dot{Z}_{VG} = \dot{C}_{17} + \dot{C}_{20}$
	$c_{13} = c_{17}$
VT	$\dot{C}_{20} + \dot{Z}_{VT} = \dot{C}_{21} + \dot{C}_{26} + \dot{C}_{70} + \dot{C}_{71} + \dot{C}_{72} + \dot{C}_{73}$
	$c_{20} = c_{21}$, $c_{20} = c_{26}$, $c_{70} = c_{71}$, $c_{70} = c_{72}$, $c_{70} = c_{73}$
IHE	$\dot{C}_{21} + \dot{C}_{24} + \dot{Z}_{IHE} = \dot{C}_{22} + \dot{C}_{25}$
	$c_{21} = c_{22}$
COND	$\dot{C}_{22} + \dot{C}_{29} + \dot{Z}_{COND} = \dot{C}_{23} + \dot{C}_{30}$
	$c_{22} = c_{23}$, $\dot{C}_{29} = 0$
FH	$\dot{C}_{25} + \dot{C}_{26} + \dot{Z}_{FH} = \dot{C}_{27}$
FP-I	$\dot{C}_{17} + \dot{C}_{67} + \dot{Z}_{FP-I} = \dot{C}_{18}$
FP-II	$\dot{C}_{15} + \dot{C}_{68} + \dot{Z}_{FP-II} = \dot{C}_{16}$
FP-III	$\dot{C}_{23} + \dot{C}_{71} + \dot{Z}_{FP-III} = \dot{C}_{24}$
FP-IV	$\dot{C}_{27} + \dot{C}_{72} + \dot{Z}_{FP-IV} = \dot{C}_{28}$
GEN-I	$\dot{C}_{14} + \dot{C}_{37} + \dot{Z}_{GEN-I} = \dot{C}_{15} + \dot{C}_{31} + \dot{C}_{38}$
	$c_{14} = c_{15}$, $(\dot{C}_{38} - \dot{C}_{37})/(\dot{E}_{38} - \dot{E}_{37}) = (\dot{C}_{31} - \dot{C}_{37})/(\dot{E}_{31} - \dot{E}_{37})$
ABS-I	$\dot{C}_{34} + \dot{C}_{40} + \dot{C}_{41} + \dot{Z}_{ABS-I} = \dot{C}_{35} + \dot{C}_{42}$
	$\dot{C}_{41} = 0$, $(\dot{C}_{34} + \dot{C}_{40})/(\dot{E}_{34} + \dot{E}_{40}) = c_{35}$
CON-I	$\dot{C}_{31} + \dot{C}_{43} + \dot{Z}_{CON-I} = \dot{C}_{32} + \dot{C}_{44}$
	$\dot{C}_{43} = 0$, $c_{31} = c_{32}$
EVA-I	$\dot{C}_{33} + \dot{C}_{45} + \dot{Z}_{EVA-I} = \dot{C}_{34} + \dot{C}_{46}$
	$\dot{C}_{45} = 0$, $c_{33} = c_{34}$
SHE-I	$\dot{C}_{36} + \dot{C}_{38} + \dot{Z}_{SHE-I} = \dot{C}_{37} + \dot{C}_{39}$
	$c_{38} = c_{39}$
SP-I	$\dot{C}_{35} + \dot{C}_{73} + \dot{Z}_{SP-I} = \dot{C}_{36}$
EV-Ia	$c_{39} = c_{40}$
EV-Ib	$c_{32} = c_{33}$

Table 5.8: Cost balance equations for each component of the system–I (continued).

Components	Cost balance equations
GEN-II	$\dot{C}_7 + \dot{C}_{53} + \dot{Z}_{GEN-II} = \dot{C}_8 + \dot{C}_{47} + \dot{C}_{54}$
	$c_7 = c_8$, $(\dot{C}_{54} - \dot{C}_{53})/(\dot{E}_{54} - \dot{E}_{53}) = (\dot{C}_{47} - \dot{C}_{53})/(\dot{E}_{47} - \dot{E}_{53})$
ABS-II	$\dot{C}_{50} + \dot{C}_{56} + \dot{C}_{57} + \dot{Z}_{ABS-II} = \dot{C}_{51} + \dot{C}_{58}$
	$\dot{C}_{57} = 0$, $(\dot{C}_{50} + \dot{C}_{56})/(\dot{E}_{50} + \dot{E}_{56}) = c_{51}$
CON-II	$\dot{C}_{47} + \dot{C}_{58} + \dot{Z}_{CON-II} = \dot{C}_{48} + \dot{C}_{60}$
	$\dot{C}_{59} = 0$, $c_{47} = c_{48}$
EVA-II	$\dot{C}_{49} + \dot{C}_{61} + \dot{Z}_{EVA-II} = \dot{C}_{50} + \dot{C}_{62}$
	$\dot{C}_{61} = 0$, $c_{49} = c_{50}$
SHE-II	$\dot{C}_{52} + \dot{C}_{54} + \dot{Z}_{SHE-II} = \dot{C}_{53} + \dot{C}_{55}$
	$c_{54} = c_{55}$
EV-IIa	$c_{55} = c_{56}$
EV-IIb	$c_{48} = c_{49}$
SP-II	$\dot{C}_{51} + \dot{C}_{69} + \dot{Z}_{SP-II} = \dot{C}_{52}$
WH	$\dot{C}_8 + \dot{C}_{10} + \dot{Z}_{WH} = \dot{C}_9 + \dot{C}_{11}$
	$\dot{C}_{10} = 0$, $c_8 = c_9$

5.2.5 Environmental analysis

The exhaust gas released into the atmosphere during the operation of a fossil fuel-based energy system is one of the primary causes of many environmental issues such as climate change and global warming. The core idea of environmental analysis is to lessen the consumption of fossil fuels, which can be accomplished by increasing the fuel conversion efficiency of a system. Estimating the amount of pollutants that an energy conversion system releases into the environment is the first and most important stage in environmental analysis. The specific CO_2 emission and environmental cost are two often used metrics for measuring the environmental impact. The quantity of CO_2 released per MWh of energy produced by an energy conversion system is defined as the specific CO_2 emission. As the definition suggests, a specific CO_2 emission only considers CO_2 released by the exhaust of a thermal system. The evaluation of specific CO_2 emission is simple and straightforward, however, the environmental cost is a more complete metric because it considers CO and NOx emersions in addition to CO_2 emissions. Both metrics are very essential in assessing environmental performance and laying the foundation for reducing environmental impact. In this chapter, the environmental cost rate is determined using the empirical relation shown in Eq. (5.21) [4].

$$\dot{C}_{env} = C_{CO}\dot{m}_{CO} + C_{CO_2}\dot{m}_{CO_2} + C_{NOx}\dot{m}_{NOx} \tag{5.21}$$

Table 5.9: Cost balance equations for each component of the system–II.

Components	Cost balance equations
AC	$\dot{C}_1 + \dot{C}_{45} + \dot{Z}_{AC} = \dot{C}_2$
	$\dot{C}_1 = 0$
APH	$\dot{C}_2 + \dot{C}_5 + \dot{Z}_{APH} = \dot{C}_3 + \dot{C}_6$
	$c_5 = c_6$
CC	$\dot{C}_3 + \dot{C}_{43} + \dot{Z}_{CC} = \dot{C}_4$
	$\dot{C}_{43} = c_f \dot{m}_f LHV$
GT	$\dot{C}_4 + \dot{Z}_{GT} = \dot{C}_5 + \dot{C}_{44} + \dot{C}_{45}$
	$c_4 = c_5$, $c_{44} = c_{45}$
HRSG	$\dot{C}_6 + \dot{C}_{15} + \dot{Z}_{HRSG} = \dot{C}_7 + \dot{C}_{12}$
	$c_6 = c_7$
ST	$\dot{C}_{12} + \dot{Z}_{ST} = \dot{C}_{13} + \dot{C}_{46} + \dot{C}_{47}$
	$c_{12} = c_{13}$, $c_{46} = c_{47}$
VG	$\dot{C}_{13} + \dot{C}_{24} + \dot{Z}_{VG} = \dot{C}_{14} + \dot{C}_{16}$
	$c_{13} = c_{14}$
VT	$\dot{C}_{16} + \dot{Z}_{VT} = \dot{C}_{17} + \dot{C}_{22} + \dot{C}_{48} + \dot{C}_{49} + \dot{C}_{50} + \dot{C}_{51}$
	$c_{16} = c_{17}$, $c_{16} = c_{22}$, $c_{48} = c_{49}$, $c_{48} = c_{50}$, $c_{48} = c_{51}$
IHE	$\dot{C}_{17} + \dot{C}_{20} + \dot{Z}_{IHE} = \dot{C}_{18} + \dot{C}_{21}$
	$c_{17} = c_{18}$
COND	$\dot{C}_{18} + \dot{C}_{25} + \dot{Z}_{COND} = \dot{C}_{19} + \dot{C}_{26}$
	$c_{18} = c_{19}$, $\dot{C}_{25} = 0$
FH	$\dot{C}_{21} + \dot{C}_{22} + \dot{Z}_{FH} = \dot{C}_{23}$
FP-I	$\dot{C}_{14} + \dot{C}_{47} + \dot{Z}_{FP-I} = \dot{C}_{15}$
FP-II	$\dot{C}_{19} + \dot{C}_{49} + \dot{Z}_{FP-II} = \dot{C}_{20}$
FP-III	$\dot{C}_{23} + \dot{C}_{50} + \dot{Z}_{FP-III} = \dot{C}_{24}$
GEN-II	$\dot{C}_7 + \dot{C}_{33} + \dot{Z}_{GEN-II} = \dot{C}_8 + \dot{C}_{27} + \dot{C}_{34}$
	$c_7 = c_8$, $(\dot{C}_{34} - \dot{C}_{33})/(\dot{E}_{34} - \dot{E}_{33}) = (\dot{C}_{27} - \dot{C}_{33})/(\dot{E}_{27} - \dot{E}_{33})$
ABS-II	$\dot{C}_{30} + \dot{C}_{36} + \dot{C}_{37} + \dot{Z}_{ABS-II} = \dot{C}_{31} + \dot{C}_{38}$
	$\dot{C}_{37} = 0$, $(\dot{C}_{30} + \dot{C}_{36})/(\dot{E}_{30} + \dot{E}_{36}) = c_{31}$
CON-II	$\dot{C}_{27} + \dot{C}_{39} + \dot{Z}_{CON-II} = \dot{C}_{28} + \dot{C}_{40}$
	$\dot{C}_{29} = 0$, $c_{27} = c_{28}$
EVA-II	$\dot{C}_{29} + \dot{C}_{41} + \dot{Z}_{EVA-II} = \dot{C}_{30} + \dot{C}_{42}$
	$\dot{C}_{41} = 0$, $c_{29} = c_{30}$
SHE-II	$\dot{C}_{32} + \dot{C}_{34} + \dot{Z}_{SHE-II} = \dot{C}_{33} + \dot{C}_{35}$
	$c_{34} = c_{35}$
EV-IIa	$c_{35} = c_{36}$
EV-IIb	$c_{28} = c_{29}$
SP-II	$\dot{C}_{31} + \dot{C}_{50} + \dot{Z}_{SP-II} = \dot{C}_{32}$
WH	$\dot{C}_8 + \dot{C}_{10} + \dot{Z}_{WH} = \dot{C}_9 + \dot{C}_{11}$
	$\dot{C}_{10} = 0$, $c_8 = c_9$

where C_{CO}, C_{CO_2} and C_{NOx} are the unit penalty costs of CO, CO_2 and NOx, respectively (C_{CO}= 0.02086 \$/kg, C_{CO_2}= 0.024 \$/kg and C_{NOx}= 6.853 \$/kg) [4] and

$\dot{m}_{CO}$, $\dot{m}_{CO_2}$ and $\dot{m}_{NOx}$ are the emission rates of CO, CO_2 and NOx, respectively.

The emission rate of CO_2 is estimated using Eq. (5.22) [28]:

$$\dot{m}_{CO_2} = x_{CO_2}\dot{m}_g \left(\frac{\bar{M}_{CO_2}}{\bar{M}_g}\right) \tag{5.22}$$

where $\bar{M}_{CO_2}$ and x_{CO_2} are the molecular weight and mole fraction of CO_2, respectively.

Table 5.10: Cost balance equations for each component of the system–III.

Components	Cost balance equations
AC	$\dot{C}_1 + \dot{C}_{39} + \dot{Z}_{AC} = \dot{C}_2$
	$\dot{C}_1 = 0$
APH	$\dot{C}_2 + \dot{C}_5 + \dot{Z}_{APH} = \dot{C}_3 + \dot{C}_6$
	$c_5 = c_6$
CC	$\dot{C}_3 + \dot{C}_{37} + \dot{Z}_{CC} = \dot{C}_4$
	$\dot{C}_{37} = c_f \dot{m}_f LHV$
GT	$\dot{C}_4 + \dot{Z}_{GT} = \dot{C}_5 + \dot{C}_{38} + \dot{C}_{39}$
	$c_4 = c_5$, $c_{38} = c_{39}$
HRSG	$\dot{C}_6 + \dot{C}_{18} + \dot{Z}_{HRSG} = \dot{C}_7 + \dot{C}_{12}$
	$c_6 = c_7$
ST	$\dot{C}_{12} + \dot{Z}_{ST} = \dot{C}_{13} + \dot{C}_{14} + \dot{C}_{40} + \dot{C}_{41} + \dot{C}_{42} + \dot{C}_{43}$
	$c_{12} = c_{13}$, $c_{12} = c_{14}$, $c_{40} = c_{41}$, $c_{40} = c_{42}$, $c_{40} = c_{43}$
COND	$\dot{C}_{14} + \dot{C}_{19} + \dot{Z}_{COND} = \dot{C}_{15} + \dot{C}_{20}$
	$c_{14} = c_{15}$, $\dot{C}_{19} = 0$
FP-I	$\dot{C}_{17} + \dot{C}_{41} + \dot{Z}_{FP-I} = \dot{C}_{18}$
FP-II	$\dot{C}_{15} + \dot{C}_{42} + \dot{Z}_{FP-II} = \dot{C}_{16}$
OWH	$\dot{C}_{16} + \dot{C}_{13} + \dot{Z}_{OWH} = \dot{C}_{17}$
GEN-II	$\dot{C}_7 + \dot{C}_{27} + \dot{Z}_{GEN-II} = \dot{C}_8 + \dot{C}_{21} + \dot{C}_{28}$
	$c_7 = c_8$, $(\dot{C}_{28} - \dot{C}_{27})/(\dot{E}_{28} - \dot{E}_{27}) = (\dot{C}_{21} - \dot{C}_{27})/(\dot{E}_{21} - \dot{E}_{27})$
ABS-II	$\dot{C}_{24} + \dot{C}_{30} + \dot{C}_{31} + \dot{Z}_{ABS-II} = \dot{C}_{25} + \dot{C}_{32}$
	$\dot{C}_{31} = 0$, $(\dot{C}_{24} + \dot{C}_{30})/(\dot{E}_{24} + \dot{E}_{30}) = c_{25}$
CON-II	$\dot{C}_{21} + \dot{C}_{33} + \dot{Z}_{CON-II} = \dot{C}_{22} + \dot{C}_{34}$
	$\dot{C}_{33} = 0$, $c_{21} = c_{22}$
EVA-II	$\dot{C}_{23} + \dot{C}_{35} + \dot{Z}_{EVA-II} = \dot{C}_{24} + \dot{C}_{36}$
	$\dot{C}_{35} = 0$, $c_{23} = c_{24}$
SHE-II	$\dot{C}_{26} + \dot{C}_{28} + \dot{Z}_{SHE-II} = \dot{C}_{27} + \dot{C}_{29}$
	$c_{28} = c_{29}$
EV-IIa	$c_{29} = c_{30}$
EV-IIb	$c_{22} = c_{23}$
SP-II	$\dot{C}_{25} + \dot{C}_{43} + \dot{Z}_{SP-II} = \dot{C}_{26}$
WH	$\dot{C}_8 + \dot{C}_{10} + \dot{Z}_{WH} = \dot{C}_9 + \dot{C}_{11}$
	$\dot{C}_{10} = 0$, $c_8 = c_9$

Table 5.11: Cost balance equations for each component of the system–IV.

Components	Cost balance equations
AC	$\dot{C}_1 + \dot{C}_{59} + \dot{Z}_{AC} = \dot{C}_2$
	$\dot{C}_1 = 0$
APH	$\dot{C}_2 + \dot{C}_5 + \dot{Z}_{APH} = \dot{C}_3 + \dot{C}_6$
	$c_5 = c_6$
CC	$\dot{C}_3 + \dot{C}_{57} + \dot{Z}_{CC} = \dot{C}_4$
	$\dot{C}_{57} = c_f \dot{m}_f LHV$
GT	$\dot{C}_4 + \dot{Z}_{GT} = \dot{C}_5 + \dot{C}_{58} + \dot{C}_{59}$
	$c_4 = c_5$, $c_{58} = c_{59}$
HRSG	$\dot{C}_6 + \dot{C}_{22} + \dot{Z}_{HRSG} = \dot{C}_7 + \dot{C}_{12}$
	$c_6 = c_7$
ST	$\dot{C}_{12} + \dot{Z}_{ST} = \dot{C}_{13} + \dot{C}_{14} + \dot{C}_{15} + \dot{C}_{60} + \dot{C}_{61} + \dot{C}_{62} + \dot{C}_{63} + \dot{C}_{64} + \dot{C}_{65}$
	$c_{12} = c_{13}$, $c_{12} = c_{14}$, $c_{12} = c_{15}$, $c_{60} = c_{61}$, $c_{60} = c_{62}$, $c_{60} = c_{63}$, $c_{60} = c_{64}$, $c_{60} = c_{65}$
COND	$\dot{C}_{15} + \dot{C}_{23} + \dot{Z}_{COND} = \dot{C}_{16} + \dot{C}_{24}$
	$c_{15} = c_{16}$, $\dot{C}_{23} = 0$
OWH	$\dot{C}_{13} + \dot{C}_{20} + \dot{Z}_{OWH} = \dot{C}_{21}$
FP-I	$\dot{C}_{21} + \dot{C}_{61} + \dot{Z}_{FP-I} = \dot{C}_{22}$
FP-II	$\dot{C}_{16} + \dot{C}_{62} + \dot{Z}_{FP-II} = \dot{C}_{17}$
FP-III	$\dot{C}_{18} + \dot{C}_{63} + \dot{Z}_{FP-III} = \dot{C}_{19}$
GEN-I	$\dot{C}_{14} + \dot{C}_{31} + \dot{Z}_{GEN-I} = \dot{C}_{18} + \dot{C}_{25} + \dot{C}_{32}$
	$c_{14} = c_{18}$, $(\dot{C}_{32} - \dot{C}_{31})/(\dot{E}_{32} - \dot{E}_{31}) = (\dot{C}_{25} - \dot{C}_{31})/(\dot{E}_{25} - \dot{E}_{31})$
ABS-I	$\dot{C}_{28} + \dot{C}_{34} + \dot{C}_{35} + \dot{Z}_{ABS-I} = \dot{C}_{29} + \dot{C}_{36}$
	$\dot{C}_{35} = 0$, $(\dot{C}_{28} + \dot{C}_{34})/(\dot{E}_{28} + \dot{E}_{34}) = c_{29}$
CON-I	$\dot{C}_{25} + \dot{C}_{37} + \dot{Z}_{CON-I} = \dot{C}_{26} + \dot{C}_{38}$
	$\dot{C}_{37} = 0$, $c_{25} = c_{26}$
EVA-I	$\dot{C}_{27} + \dot{C}_{39} + \dot{Z}_{EVA-I} = \dot{C}_{28} + \dot{C}_{40}$
	$\dot{C}_{39} = 0$, $c_{27} = c_{28}$
SHE-I	$\dot{C}_{30} + \dot{C}_{32} + \dot{Z}_{SHE-I} = \dot{C}_{31} + \dot{C}_{33}$
	$c_{32} = c_{33}$
EV-Ia	$c_{33} = c_{34}$
EV-Ib	$c_{26} = c_{27}$
SP-I	$\dot{C}_{29} + \dot{C}_{64} + \dot{Z}_{SP-I} = \dot{C}_{30}$

The emission rates of CO and NOx are estimated using Eq. (5.23) and Eq. (5.24) [2], respectively.

$$\dot{m}_{CO} = \frac{0.179 \times 10^9 exp(7800/T_{pz})}{P_3^2 \tau (\Delta P/P_3)^{0.5}} \tag{5.23}$$

$$\dot{m}_{NOx} = \frac{0.15 \times 10^{16} \tau^{0.5} exp(-71100/T_{pz})}{P_5^{0.05} (\Delta P/P_3)^{0.5}} \tag{5.24}$$

where τ is the residence time in the combustion zone which is considered as a constant and equal to 0.002 s [28] and, $\dot{m}_{CO}$ and $\dot{m}_{NOx}$ are the quantity of CO and NOx produced at the CC in grams per kg of fuel and T_{pz} is the adiabatic flame

Table 5.11: Cost balance equations for each component of the system–IV (continued).

Components	Cost balance equations
GEN-II	$\dot{C}_7 + \dot{C}_{47} + \dot{Z}_{GEN-II} = \dot{C}_8 + \dot{C}_{41} + \dot{C}_{48}$
	$c_7 = c_8$, $(\dot{C}_{48} - \dot{C}_{47})/(\dot{E}_{48} - \dot{E}_{47}) = (\dot{C}_{41} - \dot{C}_{47})/(\dot{E}_{41} - \dot{E}_{47})$
ABS-II	$\dot{C}_{44} + \dot{C}_{50} + \dot{C}_{51} + \dot{Z}_{ABS-II} = \dot{C}_{45} + \dot{C}_{52}$
	$\dot{C}_{51} = 0$, $(\dot{C}_{44} + \dot{C}_{50})/(\dot{E}_{44} + \dot{E}_{50}) = c_{45}$
CON-II	$\dot{C}_{41} + \dot{C}_{53} + \dot{Z}_{CON-II} = \dot{C}_{42} + \dot{C}_{54}$
	$\dot{C}_{53} = 0$, $c_{41} = c_{42}$
EVA-II	$\dot{C}_{43} + \dot{C}_{45} + \dot{Z}_{EVA-II} = \dot{C}_{44} + \dot{C}_{56}$
	$\dot{C}_{55} = 0$, $c_{43} = c_{44}$
SHE-II	$\dot{C}_{46} + \dot{C}_{48} + \dot{Z}_{SHE-II} = \dot{C}_{47} + \dot{C}_{49}$
	$c_{48} = c_{49}$
EV-Ia	$c_{49} = c_{50}$
EV-Ib	$c_{42} = c_{43}$
SP-II	$\dot{C}_{45} + \dot{C}_{65} + \dot{Z}_{SP-II} = \dot{C}_{46}$
WH	$\dot{C}_8 + \dot{C}_{10} + \dot{Z}_{WH} = \dot{C}_9 + \dot{C}_{11}$
	$\dot{C}_{10} = 0$, $c_8 = c_9$

temperature at the primary zone of the CC. P_3 is the CC inlet pressure and $\Delta P/P_3$ is the non-dimensional pressure drop in the CC.

The adiabatic flame temperature at the primary zone of the CC is evaluated by using the empirical relation given in Eq. (5.25) [2].

$$T_{pz} = A\sigma^{\alpha} exp\left(\beta(\sigma + \lambda)^2\right) \pi^{x^*} \theta^{y^*} \psi^{z^*} \tag{5.25}$$

where π is the dimensionless pressure (P_3/P_0), θ is the dimensionless temperature (T_3/T_0), ψ is the ratio of hydrogen to carbon atoms of the fuel, $\sigma{=}\phi$ for $\phi \leq 1$ (where ϕ is the molar ratio of fuel) and $\sigma{=}\phi - 0.7$ for $\phi \geq 1$. Further, x^*, y^* and z^* are the quadratic equations of σ shown in Eqs. (5.26) to (5.28) [2].

$$x^* = a_1 + b_1\sigma + c_1\sigma^2 \tag{5.26}$$

$$y^* = a_2 + b_2\sigma + c_2\sigma^2 \tag{5.27}$$

$$z^* = a_3 + b_3\sigma + c_3\sigma^2 \tag{5.28}$$

where the values of A, α, β, λ, a_i, b_i and c_i (where $i = 1, 2, 3$) are obtained from Ref. [2].

The specific CO_2 emission for the proposed CCHP systems are evalaued by using

Eq. (5.29) [28].

$$S_{CO_2} = \frac{\dot{m}_{CO_2}}{\dot{W}_{net} + \dot{Q}_{cooling} + \dot{Q}_{heating}} \tag{5.29}$$

where S_{CO_2} is the specific CO_2 emission in kg/MWh and $\dot{m}_{CO_2}$ is the emission rate of CO_2 in kg/h.

5.2.6 Multi-objective optimization

The multi-objective optimization of the four CCHP systems is performed by using Pareto envelope-based selection algorithm-II (PESA-II) [11]. A detailed description of PESA-II is already presented in Chapter 4 (Section 4.2.5). The PESA-II routine is linked to an in-house built MATLAB code that simulates the 4E performance of the CCHP systems. For a given set of decision variables, it then returns the Pareto optimal solutions while optimizing the objective functions simultaneously, based on the number of inequality constraints. The mathematical model for the current multi-objective optimization problem is as given below [16]:

$$\begin{cases} x = (r_p, \eta_{s,AC}, \eta_{s,GT}, T_3, P_{12}, \Delta T_{pp,HRSG})^T \\ f = (f_1(\eta_{sys}), f_2(\varepsilon_{sys}), f_2(\dot{C}_{tot}))^T \\ g_k(x) \leq 0 \colon \forall k = 1, 2, ..., j \\ 6 \leq r_p \leq 16 \\ 80\% \leq \eta_{s,AC} \leq 89\% \\ 80\% \leq \eta_{s,GT} \leq 88\% \\ 750\,\text{kPa} \leq T_3 \leq 810\,\text{K} \\ 8000\,\text{kPa} \leq P_{12} \leq 19500\,\text{kPa} \quad \text{(for system-I and system-II)} \\ 8000\,\text{kPa} \leq P_{12} \leq 11500\,\text{kPa} \quad \text{(for system-III)} \\ 8000\,\text{kPa} \leq P_{12} \leq 12000\,\text{kPa} \quad \text{(for system-IV)} \\ 20\,\text{K} \leq \Delta T_{pp,HRSG} \leq 50\,\text{K} \end{cases} \tag{5.30}$$

From Eq. (5.30), it can be observed that there are six decision variables chosen for carrying out the multi-objective optimization of the two proposed systems and they are:

- AC pressure ratio (r_p)
- Isentropic efficiency of AC ($\eta_{s,AC}$)

- Isentropic efficiency of GT ($\eta_{s,GT}$)
- APH outlet temperature (T_3)
- ST inlet pressure (P_{12})
- PPTD of HRSG ($\Delta T_{pp,HRSG}$)

The range of the decision variables is shown in Eq. (5.30). The range of r_p, $\eta_{s,AC}$, $\eta_{s,GT}$ and T_3 are determined based on Ref. [20]. The range of $\Delta T_{pp,HRSG}$ is based on Ref. [19], however, that of P_{12} is based on parametric analysis. The objective functions considered in this present study are the energy efficiency (η_{sys}), exergy efficiency (ε_{sys}) and the total cost rate ($\dot{C}_{tot}$) of the system. The energetic and the exergetic objectives are represented by η_{sys} and ε_{sys} whereas the combined objective describing the exergoeconomic and environmental aspects of the systems is $\dot{C}_{tot}$. Hence, the considered objective functions represent the 4E performance of the proposed systems. The goal of this study is to maximize energy and exergy efficiencies and to minimize the total cost rate. The objective functions are defined as follows:

- **Energy efficiency**: The energy efficiency of the overall CCHP system is given by [14, 32]:

$$\eta_{tot} = \frac{\dot{W}_{net} + \sum \dot{Q}_{ACS} + \dot{Q}_{WH}}{\dot{m}_f LHV} \tag{5.31}$$

  where $\dot{Q}_{ACS}$ is the cooling load obtained from the ACS, $\dot{Q}_{WH}$ is the process heat obtained from the WH and $\dot{W}_{net}$ is the net power obtained from the CCHP system and it is defined as follows:

$$\dot{W}_{net} = \dot{W}_{net,GT} + \dot{W}_{net,ST} + \dot{W}_{net,RR-ORC} \tag{5.32}$$

  where $\dot{W}_{net,GT}$, $\dot{W}_{net,ST}$ and $\dot{W}_{net,ORC}$ are the net power obtained from the GT cycle, ST cycle and RR-ORC, respectively.

- **Exergy efficiency**: The exergy efficiency of the CCHP system is given by [6, 14]:

$$\varepsilon_{sys} = \frac{\dot{W}_{net} + \sum \dot{Q}_{ACS}\left(1 - \frac{T_0}{T_e}\right) + \dot{Q}_{WH}\left(1 - \frac{T_0}{T_{11}}\right)}{\dot{E}_1 + \dot{E}_f} \tag{5.33}$$

  where T_e and T_{11} are the ACS's evaporator temperature and hot water temperature, respectively and $\dot{E}_f$ is the fuel exergy at the inlet to the CC.

- **Total cost rate**: The total cost rate of the systems is given by [3]:

$$\dot{C}_{tot} = \dot{C}_{sys} + \dot{C}_{env} \tag{5.34}$$

where $\dot{C}_{env}$ is the environmental cost rate and $\dot{C}_{sys}$ is the system cost rate which is defined as follows:

$$\dot{C}_{sys} = \dot{C}_f + \sum_k \dot{Z}_k + \sum_k \dot{C}_{D,k} + \dot{C}_{L,k} \tag{5.35}$$

where $\dot{C}_f$ is the fuel cost rate, $\dot{Z}_k$ is the capital investment cost rate, $\dot{C}_{D,k}$ is the exergy destruction cost rate and $\dot{C}_{L,k}$ is the exergy loss cost rate.

The constraints of the GT-HRSG cycle are based on Ref. [36] and those associated with RR-ORC are based on Ref. [31]. For the ST cycle, the dryness fraction of steam at the ST exit is limited to 0.85 [19]. Furthermore, the constraints associated with the heat exchange process in the ACS are taken into account using Ref. [30]. Meanwhile, the values of the user-defined parameters required to initiate the execution of PESA-II are provided in Chapter 4 (Table 4.7).

In this chapter, the entropy method is incorporated with the TOPSIS decision-maker [5, 8, 17] to obtain the final optimal solution from the Pareto fronts. The detailed formulation of TOPSIS is provided in Chapter 4 (Section 4.2.5). The entropy method evaluates the weights from the Pareto-optimal set and then those weights are used for executing the TOPSIS decision-maker. The weights (w_j) corresponding to each criterion is determined using the correlation given in Eq. (5.36) [18].

$$w_j = \frac{d_j}{\sum_{j=1}^{n} d_j} \tag{5.36}$$

where d_j stands for the degree of diversity, which is defined as follows [18]:

$$d_j = 1 - e_j \tag{5.37}$$

where e_j reprasents entropy value and it is evaluted using Eq. (5.38).

$$e_j = -\frac{1}{ln(m)} \sum_{i=1}^{m} p_{ij} ln(p_{ij}) \tag{5.38}$$

5.3 Results and discussion

This section presents the model validation first, followed by a discussion on the findings obtaned from 4E evaluations of four CCHP systems under a base case scenario. The performance of the CPC systems, which were previously examined in Chapter 3, is then compared with that of the CCHP systems. The outcomes of the parametric investigation are then reported. Lastly, the results obtained from the multi-objective optimization of the CCHP systems are discussed.

5.3.1 Model validation

The proposed CCHP systems are simulated using an in-house built code based on a MATLAB environment. The code's accuracy was already verified in Chapter 3 (Section 3.3.1) and Chapter 4 (Section 4.3.1) by comparing the results to data published in the literature. As the proposed systems are novel, there are no comparable system configurations to validate; therefore, the overall system model was validated by comparing the results of the individual subsystems with the existing literature separately. The validation of the GT-HRSG model was carried out with Ref. [7] (Table 3.6). Further, the ACS model and the ST cycle model were validated with Ref. [30] (Fig. 3.6) and Ref. [12] (Fig. 3.7), respectively. Lastly, the RR-ORC model is validated by comparing the results with Ref. [29] in Chapter 4 (Table 4.10).

5.3.2 4E analysis at base case

The assumptions (Section 5.2.1) and base case operating conditions outlined in Tables 5.1 to 5.3 are used to evaluate the 4E performance of the CCHP systems in this subsection. The mass flow rates and thermodynamic properties at each state point for system-I to system-IV, respectively, are shown in Tables 5.12 to 5.15. It is to be noted that each of the four CCHP systems exhibits the same state properties from state 1 to state 6, which are in fact associated with the GT cycle. It is because the operating condition of the GT plant is considered the same (refer to Table 5.1) for all four systems. The state properties for states 1-6 are thus only displayed for system-I and not for systems-II to systems-IV. Tables 5.12 to 5.15 also illustrates that the combustion gas entering the GT has the maximum temperature (1498.73 K) among all streams. The water at the exit of the expansion valve (EV-Ib and EV-IIb) above the evaporator of ACSs (ACS-I and ACS-II), meanwhile, registers the lowest temperature (278.11 K). Similar to this, the AC outlet shows the highest

pressure (1013 kPa); while the various state points of the ACSs show the lowest pressure (0.87 kPa). It is also observed that the steam generation rate (16.30 kg/s) is the same for all CCHP systems.

The power, heating and cooling outputs and energy efficiencies of the individual subsystems as well as the overall CCHP systems are shown in Table 5.16. It is observed that the GT plant in all four CCHP systems gives a fixed net power of 37.35 MW. Moreover, it is observed that the condensing type ST employed in system-III gives the highest power (18.14 MW) whereas the back-pressure type ST used in system-II generates the lowest power (13.84 MW). In system-I, 13.04 kg/s of steam is extracted from ST at a pressure of 150 kPa for driving the RR-ORC and the remaining (3.26 kg/s) is further expanded to pass through the ACS-I's generator. In system-II, the steam is also expanded up to a pressure of 150 kPa before being passed through the VG. Moreover, Table 5.16 also shows that the powers produced by the RR-ORCs in system-I and system-II are 4.15 MW and 5.55 MW, respectively. Further, it is found that system-III delivers the highest total power of 56.74 MW followed by system-II with 55.52 MW. Meanwhile, the total power generated by system-III is the next in order with 55.49 MW followed by system-IV with 54.50 MW.

Additionally,Table 5.16 shows that system-IV, out of the four systems, delivers the maximum cooling load of 16.40 MW, followed by system-I with a cooling load of 15.74 MW. It is obvious because, among the four systems, system-I and system-IV are the only systems that are incorporated with two ACSs (ACS-I and ACS-II). In system-I and system-IV, the ACS-I provides cooling loads of 5.44 MW each. The ACS-II, on the other hand, produces a cooling load of 10.30 MW, 10.44 MW, 10.86 MW, and 10.96 MW in system-I, system-II, system-III and system-IV, respectively. ACS-II delivers a significantly higher cooling load in the proposed CCHP systems than ACS-I. This is because the heat given by the exhaust gas to the ACS-II generator is substantially greater than the heat supplied by the steam to the ACS-I generator. Moreover, the WH produces 19.20 tons of hot water per hour at 353.15 K with a corresponding process heat capacity of 1.22 MW which is the same for all four systems because the inlet and outlet temperatures of the GT exhaust and water are fixed in the WH. Further, it is found that system-I delivers the maximum net energy output of 72.48 MW, followed by systems-IV, system-II, and system-III, with net energy outputs of 72.13 MW, 68.41 MW, and 67.58 MW, respectively.

Further, Table 5.16 shows that for all four CCHP systems, the energy efficiency of the GT cycle is 29.46%. Meanwhile, the energy efficiency of the ST cycle is

Table 5.12: Properties at various states points of system-I.

States	T	P	$\dot{m}$	h	s	$\dot{E}$	$\dot{C}$	c
Units	(K)	(kPa)	(kg/s)	(kJ/kg)	(kJ/kg.K)	(MW)	($/h)	($/GJ)
1	298.15	101.3	110	341.64	6.91	0.19	0.00	0.00
2	611.89	1013	110	669.72	6.99	33.74	1027.16	8.46
3	750	982.61	110	820.78	7.22	42.76	1279.40	8.31
4	1498.73	967.87	112.7	1948.76	8.07	126.35	2723.10	5.99
5	990.76	111.81	112.7	1290.27	8.19	48.34	1041.92	5.99
6	870.68	108.55	112.7	1142.80	8.04	36.76	792.22	5.99
7	490.66	105.39	112.7	701.96	7.38	9.04	194.86	5.99
8	383.15	103.33	112.7	583.78	7.12	4.66	100.33	5.99
9	373.15	101.3	112.7	572.90	7.09	4.20	90.43	5.99
10	298.15	200	5.33	105.01	0.37	0.27	0.00	0.00
11	353.15	200	5.33	335.13	1.08	0.37	10.79	8.15
12	823.15	8900	16.30	3512.94	6.82	25.00	708.22	7.87
13	384.5	150	13.04	2636.49	7.08	7.58	214.82	7.87
14	373.15	101.42	3.26	2578.17	7.09	1.69	47.84	7.87
15	373.15	101.42	3.26	419.17	1.31	0.27	7.75	7.87
16	374	8900	3.26	429.35	1.31	0.30	9.95	9.09
17	383.89	147	13.04	464.56	1.43	1.22	34.59	7.87
18	384.81	8900	13.04	474.78	1.43	1.34	42.11	8.71
19	382.65	8900	16.3	465.69	1.41	1.65	52.07	8.78
20	369	715.22	172.55	437.58	1.68	7.16	275.18	10.67
21	316.68	109.58	141.5	409.13	1.69	1.44	55.33	10.67
22	304.61	109.58	141.5	400.56	1.67	1.39	53.46	10.67
23	303.15	109.58	141.5	230.26	1.10	0.99	38.18	10.67
24	303.27	384	141.5	230.47	1.10	1.02	40.69	11.07
25	311.69	384	141.5	239.15	1.13	1.06	45.65	11.99
26	349.52	384	31.04	428.11	1.69	0.97	37.14	10.67
27	343.82	384	172.55	273.15	1.24	1.82	83.32	12.73
28	344.02	715.22	172.55	273.42	1.24	1.86	87.14	13.01
29	298.15	101.3	1152.9	104.92	0.37	0.00	0.00	–
30	303.15	101.3	1152.9	125.82	0.44	0.20	21.02	29.22
31	363.15	5.65	2.3	2669.01	8.66	0.32	12.85	10.99
32	308.15	5.65	2.3	146.63	0.51	0.12	4.61	10.99
33	278.11	0.87	2.3	146.63	0.53	0.10	4.61	12.70
34	278.15	0.87	2.3	2510.06	9.02	-0.29	-13.29	12.70
35	308.15	0.87	15.09	85.32	0.21	3.10	110.89	9.94
36	308.15	5.65	15.09	85.32	0.21	3.10	110.90	9.94
37	338.84	5.65	15.09	146.89	0.41	3.15	115.49	10.17
38	363.15	5.65	12.78	242.41	0.47	3.95	144.25	10.15
39	321.9	5.65	12.78	169.74	0.26	3.83	139.97	10.15
40	321.9	0.87	12.78	169.74	0.26	3.83	139.97	10.15

highest for system-III with 37.12% followed by system-IV with 35.09%. The energy efficiencies of the ST cycles in systems-I and system-II, however, are significantly lower, at 28.23% and 27.93%, respectively. Next, the energy efficiency of the RR-ORC in system-I and system-II are found to be 14.67% and 15.68%, respectively. Moreover, the COP of ACSs (ACS-I and ACS-II), which is the same for all four CCHP systems, is 0.774. Further, it is found that system-I has the highest energy efficiency at 57.20%, followed by system-IV (56.90%). System-II and system-III are estimated to have overall energy efficiencies of 53.96% and 53.31%, respectively.

Table 5.12: Properties at various states points of system-I (continued).

States	T	P	$\dot{m}$	h	s	$\dot{E}$	$\dot{C}$	c
Units	(K)	(kPa)	(kg/s)	(kJ/kg)	(kJ/kg.K)	(MW)	($/h)	($/GJ)
41	298.15	101.3	318.94	104.92	0.37	15.93	0.00	0.00
42	303.15	101.3	318.94	125.82	0.44	15.98	17.32	0.30
43	298.15	101.3	278.07	104.92	0.37	13.89	0.00	0.00
44	303.15	101.3	278.07	125.82	0.44	13.94	8.84	0.18
45	288.15	101.3	259.85	63.08	0.22	13.16	0.00	0.00
46	283.15	101.3	259.85	42.12	0.15	13.40	19.50	0.40
47	363.15	5.65	4.35	2669.01	8.66	0.61	29.25	13.22
48	308.15	5.65	4.35	146.63	0.51	0.22	10.49	13.22
49	278.11	0.87	4.35	146.63	0.53	0.19	10.49	15.28
50	278.15	0.87	4.35	2510.06	9.02	-0.55	-30.25	15.28
51	308.15	0.87	28.54	85.32	0.21	5.86	254.70	12.07
52	308.15	5.65	28.54	85.32	0.21	5.86	254.72	12.07
53	338.84	5.65	28.54	146.89	0.41	5.97	265.00	12.34
54	363.15	5.65	24.18	242.41	0.47	7.47	331.05	12.32
55	321.9	5.65	24.18	169.74	0.26	7.24	321.23	12.32
56	321.9	0.87	24.18	169.74	0.26	7.24	321.23	12.32
57	298.15	101.3	603.34	104.92	0.37	30.13	0.00	0.00
58	303.15	101.3	603.34	125.82	0.44	30.24	38.51	0.35
59	298.15	101.3	526.01	104.92	0.37	26.27	0.00	0.00
60	303.15	101.3	526.01	125.82	0.44	26.36	19.64	0.21
61	288.15	101.3	491.56	63.08	0.22	24.90	0.00	0.00
62	283.15	101.3	491.56	42.12	0.15	25.35	43.09	0.47
63	333.35	2650	2.7	946.87	5.1	135.60	1397.01	2.86

The exergy flow rates at each state point for system-I, system-II, system-III, and system-IV, are presented in Tables 5.12 to 5.15, respectively. The exergetic performance parameters such as exergy destruction rate ($\dot{E}_D$), exergy destruction ratio (Y_D), and exergy efficiency (ε) for each component of systems-I, system-II, system-III, and system-IV are estimated based on the calculated exergy flow rates and are shown in Tables 5.17 to 5.20, respectively. It is observed that $\dot{E}_D$ of the GT

Table 5.13: Properties at various states points of system-II.

States	T	P	$\dot{m}$	h	s	$\dot{E}$	$\dot{C}$	c
Units	(K)	(kPa)	(kg/s)	(kJ/kg)	(kJ/kg.K)	(MW)	($/h)	($/GJ)
7	491.68	105.39	112.7	703.09	7.39	9.09	195.93	5.99
8	383.15	103.33	112.7	583.78	7.12	4.66	100.33	5.99
9	373.15	101.30	112.7	572.90	7.09	4.20	90.43	5.99
10	298.15	200.00	5.33	105.01	0.37	0.27	0.00	0.00
11	353.15	200.00	5.33	335.13	1.08	0.37	10.79	8.15
12	823.15	8900.00	16.30	3512.94	6.82	25.00	707.24	7.86
13	384.50	150.00	13.04	2636.49	7.08	9.48	268.15	7.86
14	383.59	145.50	3.26	463.27	1.42	1.52	43.04	7.86
15	384.50	8900.00	3.26	473.48	1.43	1.67	52.70	8.74
16	375.00	818.48	3.26	440.74	1.69	9.31	338.27	10.09
17	318.04	109.58	13.04	410.11	1.70	1.79	65.02	10.09
18	304.75	109.58	13.04	400.65	1.67	1.72	62.47	10.09
19	303.15	109.58	16.3	230.26	1.10	1.23	44.60	10.09
20	303.27	384.00	172.55	230.47	1.10	1.26	47.51	10.47
21	312.57	384.00	141.5	240.05	1.14	1.31	53.77	11.37
22	350.88	384.00	141.5	429.18	1.69	1.16	42.16	10.09
23	343.82	384.00	141.5	273.15	1.24	2.23	96.44	12.00
24	344.08	818.48	141.5	273.51	1.24	2.30	102.07	12.32
25	298.15	101.30	141.5	104.92	0.37	0.00	0.00	–
26	302.15	101.30	31.04	121.64	0.42	0.20	24.96	35.01
27	358.15	5.65	172.55	2659.53	8.64	0.62	31.05	14.01
28	308.15	5.65	172.55	146.63	0.51	0.22	11.26	14.01
29	278.11	0.87	1152.9	146.63	0.53	0.19	11.26	16.19
30	278.15	0.87	1152.9	2510.06	9.02	-0.56	-32.49	16.19
31	308.15	0.87	2.3	85.32	0.21	7.04	276.05	10.89
32	308.15	5.65	2.3	85.32	0.21	7.04	279.94	11.05
33	338.32	5.65	2.3	145.84	0.40	7.17	291.31	11.29
34	358.15	5.65	2.3	218.36	0.46	8.81	356.60	11.24
35	320.65	5.65	15.09	149.51	0.26	8.55	345.79	11.24
36	320.65	0.87	15.09	149.51	0.26	8.55	345.79	11.24
37	298.15	101.30	15.09	104.92	0.37	30.51	0.00	0.00
38	303.15	101.30	12.78	125.82	0.44	30.62	39.56	0.36
39	298.15	101.30	12.78	104.92	0.37	26.53	0.00	0.00
40	303.15	101.30	12.78	125.82	0.44	26.62	20.70	0.22
41	288.15	101.30	318.94	63.08	0.22	25.24	0.00	0.00
42	283.15	101.30	318.94	42.12	0.15	25.70	46.12	0.50
43	333.35	2650	2.7	946.87	5.1	135.60	1397.01	2.86

plant's components are identical across all four CCHP systems. This is so because, in each of the four CCHP system configurations, the operating conditions and layouts of the GT plant are identical. The CC has the highest irreversibility among the GT

Table 5.14: Properties at various states points of system-III.

States	T	P	$\dot{m}$	h	s	$\dot{E}$	$\dot{C}$	c
Units	(K)	(kPa)	(kg/s)	(kJ/kg)	(kJ/kg.K)	(MW)	($/h)	($/GJ)
7	497.08	105.39	112.7	709.08	7.4	9.36	201.71	5.99
8	383.15	103.33	112.7	583.78	7.12	4.66	100.33	5.99
9	373.15	101.3	112.7	572.9	7.09	4.2	90.43	5.99
10	298.15	200	5.33	105.01	0.37	0.27	0	0
11	353.15	200	5.33	335.13	1.08	0.37	10.79	8.15
12	823.15	8900	16.30	3512.94	6.82	25	732.66	8.14
13	393.36	200	1.85	2679.13	7.06	1.16	34.15	8.14
14	327.12	15	14.45	2326.95	7.18	3.49	102.27	8.14
15	327.12	15	14.45	225.94	0.75	0.8	23.46	8.14
16	327.13	200	14.45	226.15	0.75	0.8	23.76	8.22
17	393.36	200	16.3	504.7	1.53	1.68	74.22	12.28
18	394.33	8900	16.3	514.94	1.53	1.83	84.21	12.76
19	298.15	101.3	1452.5	104.92	0.37	72.54	0	0
20	303.15	101.3	1452.5	125.82	0.44	72.8	84.29	0.32
21	358.15	5.65	4.59	2659.53	8.64	0.64	30.1	13.05
22	308.15	5.65	4.59	146.63	0.51	0.23	10.92	13.05
23	278.11	0.87	4.59	146.63	0.53	0.2	10.92	15.08
24	278.15	0.87	4.59	2510.06	9.02	-0.58	-31.5	15.08
25	308.15	0.87	37.98	85.32	0.21	7.33	304.82	11.56
26	308.15	5.65	37.98	85.32	0.21	7.33	304.84	11.56
27	338.32	5.65	37.98	145.84	0.4	7.46	317.22	11.81
28	358.15	5.65	33.38	218.36	0.46	9.17	389.24	11.79
29	320.65	5.65	33.38	149.51	0.26	8.9	377.45	11.79
30	320.65	0.87	33.38	149.51	0.26	8.9	377.45	11.79
31	298.15	101.3	635.94	104.92	0.37	31.76	0	0
32	303.15	101.3	635.94	125.82	0.44	31.87	43.5	0.38
33	298.15	101.3	552.82	104.92	0.37	27.61	0	0
34	303.15	101.3	552.82	125.82	0.44	27.71	20.11	0.2
35	288.15	101.3	518.56	63.08	0.22	26.27	0	0
36	283.15	101.3	518.56	42.12	0.15	26.75	44.84	0.47
37	333.35	2650	2.7	946.87	5.1	135.6	1397.01	2.86

cycle components, with $\dot{E}_D$ of 52.01 MW, followed by the GT and APH. In fact, among all the components of system-I, system-II, system-III, and system-IV, CC has the highest $\dot{E}_D$. The presence of significant irreversibility, primarily as a result of the combustion reaction, is the cause of the high $\dot{E}_D$. Tables 5.12 to 5.15 shows that CC alone accounts for 70.65%, 71.50%, 70.35% and 69.74% of the overall exergy destruction rate corresponding to system-I, system-II, system-III and system-IV, respectively.

The HRSG is the next major source of $\dot{E}_D$ in the CCHP systems. The $\dot{E}_D$ of HRSG in system-I, system-II, system-III and system-IV are 4.37 MW, 4.35 MW, 4.24 MW and 4.24 MW, respectively with Y_D of 5.93%, 5.98%, 5.73% and 5.67%. The HRSG's high $\dot{E}_D$ is caused by fluid friction and heat transfer, with stream-to-stream heat transfer being the dominant contributor to irreversibility. The GT has the third-highest $\dot{E}_D$ (3.82 MW) in all four CCHP systems. Moreover, Y_D of

Table 5.15: Properties at various states points of system-IV.

States	T	P	$\dot{m}$	h	s	$\dot{E}$	$\dot{C}$	c
Units	(K)	(kPa)	(kg/s)	(kJ/kg)	(kJ/kg.K)	(MW)	($/h)	($/GJ)
7	497.08	105.39	112.70	709.08	7.40	9.26	199.89	5.99
8	383.15	103.33	112.70	583.78	7.12	4.56	98.38	5.99
9	373.15	101.30	112.70	572.90	7.09	4.10	88.47	5.99
10	298.15	200.00	5.33	105.01	0.37	0.27	0.00	0.00
11	353.15	200.00	5.33	335.13	1.08	0.37	10.80	8.16
12	823.15	8900.00	16.30	3512.94	6.82	25.00	743.89	8.27
13	393.36	200.00	2.44	2679.13	7.06	1.54	45.80	8.27
14	373.15	101.42	3.26	2576.48	7.09	1.69	50.22	8.27
15	327.12	15.00	3.26	2325.68	7.17	2.56	76.10	8.27
16	327.12	15.00	3.26	225.94	0.75	0.59	17.47	8.27
17	327.13	200.00	10.59	226.15	0.75	0.59	17.70	8.35
18	373.15	101.42	3.26	419.17	1.31	0.27	8.14	8.27
19	373.16	200.00	3.26	419.28	1.31	0.27	8.20	8.31
20	337.99	200.00	13.85	271.59	0.89	0.84	25.90	8.61
21	393.36	200.00	16.30	504.70	1.53	1.68	84.52	13.98
22	394.33	8900.00	16.30	514.94	1.53	1.83	94.70	14.35
23	298.15	101.30	1064.40	104.92	0.37	53.16	0.00	0.00
24	303.15	101.30	1064.40	125.82	0.44	53.35	62.91	0.33
25	363.15	5.65	2.30	2669.01	8.66	0.32	13.45	11.51
26	308.15	5.65	2.30	146.63	0.51	0.12	4.82	11.51
27	278.11	0.87	2.30	146.63	0.53	0.10	4.82	13.30
28	278.15	0.87	2.30	2510.06	9.02	-0.29	-13.91	13.30
29	308.15	0.87	15.08	85.32	0.21	3.10	116.22	10.43
30	308.15	5.65	15.08	85.32	0.21	3.10	116.23	10.43
31	338.84	5.65	15.08	146.89	0.41	3.15	121.03	10.67
32	363.15	5.65	12.77	242.41	0.47	3.94	151.17	10.65
33	321.90	5.65	12.77	169.74	0.26	3.83	146.69	10.65
34	321.90	0.87	12.77	169.74	0.26	3.83	146.69	10.65
35	298.15	101.30	318.71	104.92	0.37	15.92	0.00	0.00
36	303.15	101.30	318.71	125.82	0.44	15.97	18.07	0.31
37	298.15	101.30	277.86	104.92	0.37	13.88	0.00	0.00
38	303.15	101.30	277.86	125.82	0.44	13.93	9.23	0.18
39	288.15	101.30	259.66	63.08	0.22	13.16	0.00	0.00

Table 5.15: Properties at various states points of system-IV (continued).

States	T	P	$\dot{m}$	h	s	$\dot{E}$	$\dot{C}$	c
Units	(K)	(kPa)	(kg/s)	(kJ/kg)	(kJ/kg.K)	(MW)	($/h)	($/GJ)
40	283.15	101.30	259.66	42.12	0.15	13.39	20.34	0.42
41	358.15	5.65	4.64	2659.53	8.64	0.65	30.14	12.95
42	308.15	5.65	4.64	146.63	0.51	0.23	10.93	12.95
43	278.11	0.87	4.64	146.63	0.53	0.20	10.93	14.96
44	278.15	0.87	4.64	2510.06	9.02	-0.59	-31.54	14.96
45	308.15	0.87	38.32	85.32	0.21	7.39	305.21	11.47
46	308.15	5.65	38.32	85.32	0.21	7.39	305.23	11.47
47	338.32	5.65	38.32	145.84	0.40	7.53	317.63	11.72
48	358.15	5.65	33.68	218.36	0.46	9.26	389.74	11.69
49	320.65	5.65	33.68	149.51	0.26	8.98	377.93	11.69
50	320.65	0.87	33.68	149.51	0.26	8.98	377.93	11.69
51	298.15	101.30	641.68	104.92	0.37	32.05	0.00	0.00
52	303.15	101.30	641.68	125.82	0.44	32.16	43.56	0.38
53	298.15	101.30	557.80	104.92	0.37	27.86	0.00	0.00
54	303.15	101.30	557.80	125.82	0.44	27.96	20.14	0.20
55	288.15	101.30	523.23	63.08	0.22	26.51	0.00	0.00
56	283.15	101.30	523.23	42.12	0.15	26.99	44.91	0.46
57	333.35	2650.00	2.70	946.87	5.10	135.60	1397.01	2.86

Table 5.16: Energy outputs of the four CCHP systems.

Parameters	Units	System-I	System-II	System-III	System-IV
Net GT power	MW	37.35	37.35	37.35	37.35
Net ST power	MW	14.02	13.84	18.14	17.15
Net RR-ORC power	MW	4.15	5.55	–	–
Net power	MW	55.52	56.74	55.49	54.50
Process heat	MW	1.22	1.22	1.22	1.22
ACS-I cooling output	MW	5.44	–	–	5.44
ACS-II cooling output	MW	10.30	10.44	10.86	10.96
Net cooling output	MW	15.74	10.44	10.86	16.40
Net output energy	MW	72.48	68.41	67.58	72.13
Energy efficiency of GT cycle	%	29.46	29.46	29.46	29.46
Energy efficiency of ST cycle	%	28.23	27.93	37.12	35.09
Energy efficiency of RR-ORC	%	14.67	15.68	–	–
COP of ACS-I	–	0.774	–	–	0.774
COP of ACS-II	–	0.774	0.774	0.774	0.774
Overall energy efficiency	%	57.20	53.96	53.31	56.90

GT in system-I, system-II, system-III and system-IV are 5.19%, 5.25%, 5.17% and 5.11%, respectively. The fluid friction that occurs when combustion gas impinges on the turbine blades is the primary cause of exergy destruction in the GT. The

APH and AC are the next major source of irreversibility in the CCHP systems with $\dot{E}_D$ of 2.57 MW and 2.54 MW, respectively. The GEN-II appears next in the list with $\dot{E}_D$ in system-I, system-II, system-III and system-IV are 2.27 MW, 2.18 MW, 2.35 MW and 2.33 MW, respectively. The irreversibilities generated by the heat transfer between the flue gas and the LiBr-H_2O solution and the separation of H_2O from the LiBr-H_2O solution are the source of substantial exergy destruction in GEN-II. It is interesting to note that $\dot{E}_D$ in the condensing type STs (system-III and system-IV) are higher than that of back-pressure type STs (system-I and system-II). It is because, in the condensing type STs, the steam is expanded up to a very low pressure (condenser pressure) which results in higher irreversibilities associated with the fluid friction.

Table 5.17 and Table 5.18 also shows that among the RR-ORC components (system-I and system-II), VG has $\dot{E}_D$ followed by VT. It is also interesting to observe that $\dot{E}_D$ in CONDs of RR-ORCs (system-I and system-II) is significantly less than that of the CONDs of the ST cycle (system-III and system-IV). Moreover, in condensing type STs, the OWH has a marginal $\dot{E}_D$ of 0.29 MW and 0.70 MW in system-III and system-IV, respectively. The reason for higher $\dot{E}_D$ in the OWH of system-IV is due to a higher mass flow rate of extracted steam as compared to system-III. Moreover, it is intriguing to note that the components of ACS-I show the same pattern of $\dot{E}_D$ in all four systems. The largest $\dot{E}_D$ among the ACS-I components is incurred by ABS-I, followed by GEN-I, CON-I, EVA-I, and SHE-I. Particularly, in system-I, the ABS-I has an $\dot{E}_D$ of 0.39 MW and $\dot{E}_D$ of GEN-I, CON-I, EVA-I, and SHE-I are 0.30 MW, 0.16 MW, 0.15 MW and 0.06 MW, respectively. In system-IV also the respective ACS-I's components have the same $\dot{E}_D$. It is because the cooling load obtained from the ACS-I of both the systems (system-I and system-IV) is the same (5.44 MW). Moreover, the exothermic reaction is the reason for the higher $\dot{E}_D$ in the ACS-I's absorber. On the other hand, Tables 5.17 to 5.20 shows that the largest $\dot{E}_D$ among the ACS-II components is incurred by GEN-II, followed by ABS-II, CON-II, EVA-II, and SHE-II. The $\dot{E}_D$ rate of GEN-II in system-II and system-III is 2.18 MW and 2.35 MW, respectively.

From Tables 5.17 to 5.20, it is observed that GT is the most efficient component in all four systems with the highest exergy efficiency of 95.10%. The next most efficient component is the AC with exergy efficiency of 92.95%. In the topping GT plant, the CC has the least exergy efficiency of 70.84%. It is justified because, in the CC, the majority of the fuel exergy is destroyed due to the presence of irreversibilities, which ultimately lowers exergy efficiency. A general observation can

also be drawn from Tables 5.17 to 5.20 that the heat exchangers have lower exergy efficiency. For instance, the condenser, IHE and all the components of ACSs show very poor exergy efficiency. In fact, the absorber of ACS-II shows the least exergy efficiency of 12.53% in all four systems.

Table 5.17: Exergy and exergoeconomic performance of the components of system-I.

Components	$\dot{E}_D$	Y_D	ε	$\dot{C}_D$	$\dot{Z}_k$	$\dot{C}_D + \dot{Z}_k$	r_k	f_k
Units	MW	%	%	\$/h	\$/h	\$/h	%	%
AC	2.54	3.45	92.95	55.3	149.12	204.42	25.85	72.95
APH	2.57	3.49	77.85	61.86	2.54	64.4	29.76	3.94
CC	52.01	70.65	70.84	780.41	46.69	827.1	43.62	5.65
GT	3.82	5.19	95.1	82.31	105.57	187.88	11.75	56.19
HRSG	4.37	5.93	84.24	94.12	58.79	152.91	30.39	38.45
ST	1.25	1.7	92.03	35.52	78.13	113.65	27.72	68.75
FP-I	0.01	0.01	92.25	0.38	2.61	2.99	66.01	87.29
FP-II	≈ 0	≈ 0	92.03	0.1	0.97	1.07	95.07	90.65
FP-III	≈ 0	≈ 0	90.17	0.16	0.9	1.06	73.17	84.91
FP-IV	≈ 0	0.01	91.33	0.22	1.25	1.47	63.19	85.03
VG	1.06	1.44	83.37	29.98	7.81	37.79	25.15	20.67
VT	0.44	0.6	90.77	9.46	45.78	55.24	37.78	82.87
IHE	0.01	0.02	76.44	0.44	3.1	3.54	247.2	87.57
COND	0.2	0.27	50.23	8.48	0.53	9.01	12.12	5.88
FH	0.21	0.28	89.76	7.6	5.74	13.34	173.9	43.03
GEN-I	0.3	0.4	78.99	8.42	1.52	9.94	31.41	15.29
ABS-I	0.39	0.52	12.53	13.81	1.53	15.34	775.05	9.97
CON-I	0.16	0.22	23.13	7.00	0.59	7.59	363.6	7.77
EVA-I	0.15	0.21	60.91	6.34	1.6	7.94	78.89	20.15
SHE-I	0.06	0.08	48.05	2.22	0.31	2.53	123.2	12.25
GEN-II	2.27	3.09	48.2	48.97	0.78	49.75	109.18	1.57
ABS-II	0.73	0.99	12.53	31.72	2.24	33.96	747.16	6.6
CON-II	0.3	0.41	23.13	14.43	0.87	15.3	352.49	5.69
EVA-II	0.29	0.39	60.91	15.93	2.35	18.28	73.65	12.86
SHE-II	0.12	0.16	48.05	5.1	0.45	5.55	117.75	8.11
WH	0.36	0.49	22	17.72	0.89	18.61	395.68	4.78
system-I	73.61	–	41.87	1338	522.71	1860.66	–	33.28

The exergoeconomic performance parameters such as exergy destruction cost rate ($\dot{C}_D$), capital investment cost rate ($\dot{Z}_k$), relative cost difference (r_k) and exergoeconomic factor (f_k) for each component of systems-I, system-II, system-III, and system-IV are estimated based on the calculated cost flow rates and are shown in Tables 5.17 to 5.20, respectively. It is noted that $\dot{C}_D$ of the GT plant's components are the same across all four CCHP systems. This is so because, in each of the four CCHP system configurations, the GT cycle components have the same exergy de-

Table 5.18: Exergy and exergoeconomic performance of the components of system-II.

Components	$\dot{E}_D$	Y_D	ε	$\dot{C}_D$	$\dot{Z}_k$	$\dot{C}_D + \dot{Z}_k$	r_k	f_k
Units	MW	%	%	\$/h	\$/h	\$/h	%	%
AC	2.54	3.50	92.95	55.30	149.12	204.42	25.85	72.95
APH	2.57	3.53	77.85	61.86	2.54	64.41	29.76	3.95
CC	52.01	71.50	70.84	780.41	46.69	827.10	43.62	5.65
GT	3.82	5.25	95.10	82.31	105.57	187.89	11.75	56.19
HRSG	4.35	5.98	84.29	93.66	58.25	151.91	30.22	38.35
ST	1.24	1.70	92.03	34.99	116.16	151.15	37.40	76.85
FP-I	0.01	0.02	92.24	0.51	3.06	3.57	58.68	85.67
FP-II	≈ 0	≈ 0	90.17	0.18	1.05	1.23	73.26	85.12
FP-III	0.01	0.01	91.33	0.34	1.76	2.09	59.28	83.99
VG	0.95	1.30	88.11	26.77	11.09	37.86	19.09	29.29
VT	0.58	0.80	90.84	12.56	56.15	68.70	36.83	81.72
IHE	0.02	0.02	75.66	0.62	3.71	4.33	224.59	85.67
COND	0.24	0.33	90.19	9.41	0.51	9.92	11.47	5.16
FH	0.29	0.40	40.27	10.67	7.09	17.76	246.95	39.93
GEN-II	2.18	2.99	50.94	46.90	0.73	47.63	97.81	1.54
ABS-II	0.84	1.16	11.15	33.10	2.30	35.40	852.62	6.51
CON-II	0.30	0.41	23.47	17.10	0.91	18.01	345.68	5.04
EVA-II	0.29	0.40	60.91	15.15	2.37	17.51	73.07	13.52
SHE-II	0.14	0.19	48.75	5.54	0.57	6.11	115.99	9.37
WH	0.36	0.49	22.00	17.72	0.89	18.61	395.68	4.78
system-II	72.73	–	42.48	1305.10	570.55	1875.70	–	29.16

struction rates. Moreover, among all the components of the CCHP systems, CC has the highest $\dot{C}_D$ of 780.41 \$/h. The presence of significant irreversibility due to combustion reaction is once again the cause of the high $\dot{C}_D$. The $\dot{Z}_k$ for AC in system-I and system-II is found to be the highest among all the components. While ST is found to have the greatest $\dot{Z}_k$ among all the components in system-III and system-IV. However, $\dot{Z}_k$ of ST in system-I and system-II is comparatively less. It shows that $\dot{Z}_k$ of a condensing type ST (system-III and system-IV) is higher than that of the back-pressure type of ST (system-I and system-II).The PEC_k for the components of the CCHP layouts are presented in Table A.2 (refer to Appendix).

The CC has the highest value of $\dot{C}_D + \dot{Z}$ in all four systems. It suggests that, from an exergoeconomic perspective, CC is the most crucial component. It can also be observed that f_k of CC is significantly low (5.65%) in all four systems. It implies that the majority of the cost associated with CC is due to exergy destruction. The cost-effectiveness of overall systems can be increased by improving the combustion efficiency of the CC which would lower $\dot{C}_D$ with a manageable increase in $\dot{Z}_k$. This

Table 5.19: Exergy and exergoeconomic performance of the components of system-III.

Components	$\dot{E}_D$	Y_D	ε	$\dot{C}_D$	$\dot{Z}_k$	$\dot{C}_D + \dot{Z}_k$	r_k	f_k
Units	MW	%	%	\$/h	\$/h	\$/h	%	%
AC	2.54	3.44	92.95	55.30	149.12	204.42	25.85	72.95
APH	2.57	3.47	77.85	61.86	2.54	64.41	29.76	3.95
CC	52.01	70.35	70.84	780.41	46.69	827.10	43.62	5.65
GT	3.82	5.17	95.10	82.31	105.57	187.89	11.75	56.19
HRSG	4.24	5.73	84.54	91.29	57.94	149.23	29.89	38.83
ST	1.67	2.26	91.80	48.87	164.30	213.17	38.94	77.07
FP-I	0.01	0.02	92.44	0.52	3.06	3.59	56.04	85.40
FP-II	≈ 0	≈ 0	90.89	0.01	0.18	0.19	165.93	93.96
OWH	0.29	0.39	85.31	8.51	16.31	24.82	50.24	65.72
COND	2.44	3.30	9.36	71.43	5.48	76.91	1042.28	7.13
GEN-II	2.35	3.18	50.00	50.69	0.74	51.43	101.46	1.44
ABS-II	0.88	1.19	11.15	36.55	2.36	38.91	848.60	6.07
CON-II	0.31	0.42	23.47	14.68	0.93	15.61	346.78	5.95
EVA-II	0.31	0.41	60.91	16.58	2.43	19.01	73.58	12.76
SHE-II	0.14	0.19	48.75	6.04	0.59	6.63	115.32	8.84
WH	0.36	0.48	22.00	17.72	0.89	18.61	395.68	4.80
system-III	73.92	–	41.58	1342.80	559.16	1901.90	–	28.20

can be accomplished by increasing the temperature of the reactant (air and fuel) at the inlet to the CC [7]. The AC is the second most critical component in system-I and system-II with the respective $\dot{C}_D + \dot{Z}$ values of 204.42 \$/h each. On the other hand, ST is the second most critical component in system-III and system-IV with the respective $\dot{C}_D + \dot{Z}$ values of 213.17 \$/h and 212.65 \$/h. The f_k of AC in system-I and system-II is 72.95%. It indicates that a major fraction of the cost associated with the AC in both systems is caused by $\dot{Z}_k$. Similarly, f_k of ST in system-III and system-IV is 77.07% and 78.35%, respectively. The $\dot{Z}_k$ of AC can be reduced at the expanse of increased $\dot{C}_D$ by decreasing at least one or both the key variables: pressure ratio (P_2/P_1) and isentropic efficiency (η_{AC}) [7]. Similarly, $\dot{Z}_k$ of ST can be reduced at the expanse of increased $\dot{C}_D$ by decreasing isentropic efficiency (η_{ST}), steam inlet temperature (T_{12}) and steam extraction pressure [7].

The GT is the next most crucial component in system-I and system-II with the $\dot{C}_D + \dot{Z}$ value of 187.88 \$/h. The f_k of GT is 56.19% in both the systems which indicates that the cost-effectiveness of the overall systems will improve if $\dot{Z}_k$ is reduced modestly. It can be achieved by adjusting the key parameters such as CC outlet temperature (T_4), isentropic efficiency (η_{GT}) and expansion pressure ratio (P_4/P_5) [7]. The third most important component in system-III and system-IV,

Table 5.20: Exergy and exergoeconomic performance of the components of system-IV.

Components	$\dot{E}_D$	Y_D	ε	$\dot{C}_D$	$\dot{Z}$	$\dot{C}_D + \dot{Z}$	r	f
Units	MW	%	%	\$/h	\$/h	\$/h	%	%
AC	2.54	3.40	92.95	55.30	149.12	204.42	25.83	72.95
APH	2.57	3.43	77.85	61.86	2.54	64.40	29.76	3.95
CC	52.10	69.74	70.79	780.41	46.69	827.10	43.73	5.65
GT	3.82	5.11	95.10	82.31	105.57	187.88	11.74	56.19
HRSG	4.24	5.67	84.54	91.41	57.94	149.35	29.88	38.80
ST	1.55	2.07	91.95	46.04	166.61	212.65	40.45	78.35
FP-I	0.01	0.02	92.44	0.54	3.06	3.60	54.81	85.07
FP-II	≈ 0	≈ 0	90.89	0.01	0.14	0.15	176.24	94.31
FP-III	≈ 0	≈ 0	92.01	≈ 0	0.04	0.04	283.75	96.94
OWH	0.70	0.93	70.72	20.99	12.83	33.82	66.70	37.93
COND	1.79	2.39	9.36	53.15	4.27	57.42	1045.85	7.44
GEN-I	0.30	0.40	78.99	8.84	1.52	10.36	31.17	14.69
ABS-I	0.39	0.52	12.53	14.48	1.52	16.00	771.48	9.53
CON-I	0.16	0.21	23.13	7.32	0.59	7.92	362.19	7.51
EVA-I	0.15	0.20	60.91	6.63	1.60	8.24	78.22	19.45
SHE-I	0.06	0.08	48.05	2.33	0.31	2.64	122.50	11.75
GEN-II	2.33	3.12	50.45	50.30	0.74	51.04	99.66	1.45
ABS-II	0.89	1.19	11.15	36.60	2.37	38.97	848.82	6.09
CON-II	0.32	0.42	23.47	16.60	0.93	17.54	346.87	5.33
EVA-II	0.31	0.41	60.91	14.70	2.44	17.14	73.61	14.23
SHE-II	0.14	0.19	48.75	6.05	0.59	6.64	115.36	8.88
WH	0.36	0.48	22.00	17.73	0.89	18.62	395.63	4.80
system-IV	74.70	–	41.14	1375.70	562.34	1938	–	27.88

however, is the AC, followed by the GT. It can also be observed that in all four systems, HRSG also has high values of $\dot{C}_D + \dot{Z}$ with an f_k of around 38%. It implies that in HRSG, $\dot{C}_D$ outweighs $\dot{Z}_k$. As a result, lowering $\dot{C}_D$ could be cost-effective for all four systems.

Among the components of RR-ORC (system-I and system-II), VT has the highest $\dot{C}_D + \dot{Z}$ value with a significantly high f_k of around 81%. It suggests that it could be cost-effective to minimize $\dot{Z}_k$ of the VT by adjusting the isentropic efficiency (η_{VT}). As recommended in Ref. [7], special attention is required to be given to components with very high r_k. It is suggested that the higher the value of r_k, the greater the potential for improving the cost-effectiveness of the overall system. Among the RR-ORC components, IHE has a very high r_k in both systems (system-I and system-II). Also, f_k of IHE is very higher which indicates that $\dot{Z}_k$ of IHE should be reduced. On the other hand, f_k of COND in the RR-ORC is relatively lower. It

indicates that an attempt should be made to reduce the exergy destruction in the COND. The same is true for the COND of the ST cycle (system-III and system-IV). Moreover, among the components of ACSs (ACS-I and ACS-II), GEN-II has the highest $\dot{C}_D + \dot{Z}$ value with a significantly low f_k of around 1.5%. In fact, f_k of GEN-II is the lowest among all the components of the CCHP systems. Therefore, measures need to be taken to reduce the exergy destruction at the GEN-II even at the expanse of increased $\dot{Z}_k$ to improve the cost-effectiveness of the overall systems.

Table 5.21: Exergy, exergoeconomic and environmental performance of the CCHP systems.

Parameters	Units	System-I	System-II	System-III	System-IV
Exergy destruction rate	MW	73.61	72.73	73.92	74.7
Exergy efficiency	%	41.87	42.48	41.58	41.14
Exergy loss rate	MW	4.2	4.2	4.2	4.2
Fuel cost rate	$/h	1397	1397	1397	1397
Exergy loss cost rate	$/h	80.43	80.43	80.43	80.43
Exergy destruction cost rate	$/h	1338	1305.1	1342.8	1375.7
Capital investment cost rate	$/h	522.71	570.55	559.16	562.34
System cost rate	$/h	3338.2	3353.1	3379.4	3413.5
Exergoeconomic factor	%	33.28	29.16	28.2	27.88
Environmental cost rate	$/h	477.27	477.27	477.27	477.27
Specific CO_2 emission	kg/MWh	93.57	99.17	100.39	94.05
Total cost rate	$/h	3815.4	3830.4	3856.7	3890.8

Table 5.21 displays the overall exergy, exergoeconomic and environmental performance of the four CCHP systems. It is observed that system-II has the lowest exergy destruction rate of 72.73 MW among the CCHP systems. As a result, system-II is found to have the highest exergy efficiency, at 42.48%. Moreover, the exergy lost to the ambient with the exhaust gas leaving the WH is the same (4.2 MW) for all four systems. It is because the temperature, pressure, and mass flow rate of exhaust gas at the stack (state 9) are the same for all the CCHP systems. Further, it can be seen that the fuel cost rate is the same for all the systems owing to the same fuel flow rates. The exergy loss cost rate for all systems is found to be the same due to equal exergy loss rates. Moreover, system-II has the lowest exergy destruction cost rate at 1305.1 $/h due to the lowest irreversibility compared to the other systems. However, system-II has the highest capital investment cost rate at 570.55 $/h, whereas system-I has the lowest at 522.71 $/h. Furthermore, the system cost rate is also found to be lower for system-I, at 3338.62 $/h. Similarly, system-I also has the highest exergoeconomic factor (33.28%), while System-IV has the lowest (27.88%). Furthermore, the environmental cost rate for all four systems is shown

to be the same (477.27 $/h). It is because the environmental cost rate is primarily controlled by the fuel flow rate and adiabatic flame temperature, both of which are set the same for all four systems. On the other hand, even though the rate of CO_2 emissions is the same for all four systems, system-I has the lowest (93.57 kg/MWh) specific CO_2 emission since it generates the highest net energy output. Finally, the total cost rate for system-I is found to be the lowest among all the CCHP systems with 3815.4 $/h.

5.3.3 Comparative study

The four new CCHP system configurations proposed in this chapter are modifications of four similar CPC systems proposed earlier in Chapter 3. The modifications made to a given system must offer benefits in terms of superior performance over the previous one then only the modifications are justified. So to assess the performance benefits, additionally, in this chapter, the performances of the CCHP systems are compared with the previously proposed CPC systems. For unbiased comparison, the objective functions; energy efficiency, exergy efficiency and total cost rate for both CPC and CCHP systems are evaluated at the same base case condition. Table 5.22 shows that all four configurations of CCHP systems have higher energy and exergy efficiencies compared to their CPC counterparts. The total cost rates of the CPC systems, which were not calculated earlier in Chapter 3, are also computed to compare the exergoeconomic and environmental performance. Table 5.22 shows that the total cost rates of the CCHP systems are significantly less than that of CPC systems. In fact, the total cost rate of system-I reduces by 24.67%. It is found that the main reason for the decrease in total cost rates of the CCHP systems is the reduction in the exergy destruction cost rates. This supports the claim that the changes made to CPC systems to convert them to CCHP systems have improved the overall performance and made the systems more cost-effective.

Table 5.22: Performance comparison of the CCHP systems with CPC systems.

Systems	η_{tot} (%)			ε_{tot} (%)			$\dot{C}_{tot}$ ($/h)		
	CPC	CCHP	Δ (%)	CPC	CCHP	Δ (%)	CPC	CCHP	Δ(%)
System-I	56.31	57.2	+1.58	36.29	41.87	+15.37	5065	3815.4	-24.67
System-II	47.98	53.96	+12.46	37.45	42.48	+13.43	4812.9	3830.4	-20.41
System-III	47.76	53.31	+11.62	37.6	41.58	+10.58	4838.2	3856.7	-20.28
System-IV	56.03	56.9	+1.01	36.91	41.14	+11.46	5046	3890.8	-22.89

5.3.4 Parametric results

In this section, the impact of changing the AC pressure ratio (r_p), isentropic efficiency of AC ($\eta_{s,AC}$), isentropic efficiency of GT ($\eta_{s,GT}$), APH outlet temperature (T_3), ST inlet pressure (P_{12}), and PPTD of HRSG ($\Delta T_{pp,HRSG}$) on the proposed CCHP systems' energy efficiency (ε_{tot}), exergy efficiency (η_{tot}), and total cost rate ($\dot{C}_{tot}$) are discussed. The parametric assessment for a given operating condition is carried out by varying that specific operating condition within the given range while maintaining the other operating conditions fixed at their respective base case condition values (see Tables 5.1 to 5.3).

AC pressure ratio

As r_p, the air pressure (P_2) at the AC outlet rises as well, increasing the compression work. In the meantime, the pressure (P_4) of combustion gas at the inlet of GT also increases which increases the power obtained from the turbine. The rate of increase in GT power, however, is greater than the rate of increase in compression work, which increases net GT power. Additionally, it is noted that in general, the temperature (T_6) of the flue gas at the HRSG inlet decreases as r_p rises. It reduces the amount of heat recovered at the HRSG, which lowers the rate of steam generation ($\dot{m}_s$) and consequently lowers the net power obtained from the ST. It is also observed that the net power obtained from the RR-ORCs of systems-I and systems-II decreases. It is because the heat source of RR-ORCs is the wet steam extracted from the STs and with the decrease in $\dot{m}_s$, the mass flow rate of extracted steam also decreases. In fact for the same reason, the cooling output of the ACS-I in system-I and system-IV decreases. Since the wet steam extracted from the ST is utilized as a heat source for driving the ACS-I in both system-I and system-IV. On the other hand, the cooling output obtained from the ACS-II in all four CCHP systems increases with the increase in r_p. It is because as r_p increases, the flue gas temperature (T_7) at the inlet of ACS-II's generator also increases. Moreover, the flue gas temperature (T_8) at the outlet of ACS-II's generator is maintained fixed at 383.15 K, therefore the heat available for the operation of ACS-II increases resulting increase in cooling output. In general, it is seen that as r_p rises, the net energy output from all CCHP systems also increases.

The effect of change in r_p on the energy efficiency (η_{tot}), exergy efficiency (ε_{tot}), and total cost rate ($\dot{C}_{tot}$) of the four CCHP systems are depicted in Figs. 5.5(a) to 5.5(c), respectively. The upper limit of the AC pressure ratio is set at 16, while

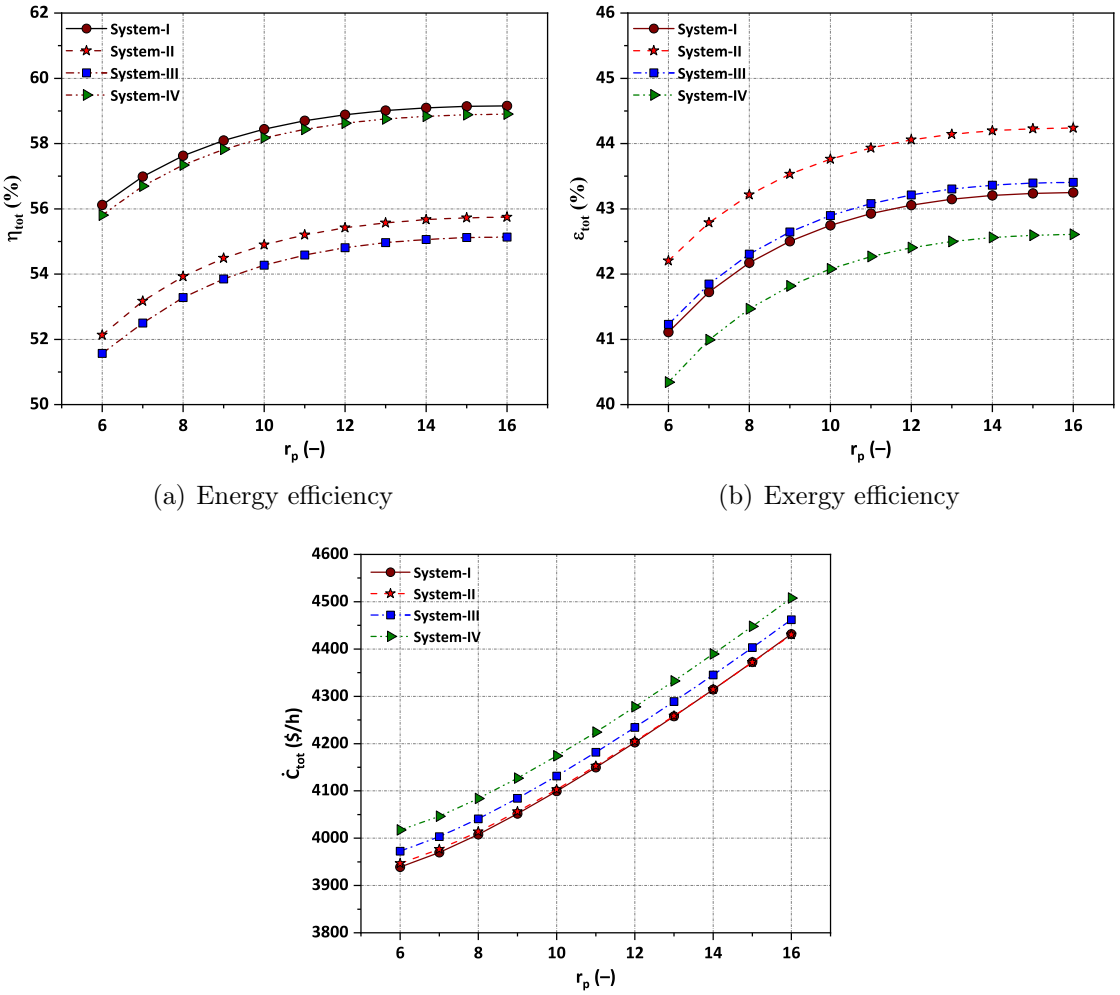

(a) Energy efficiency

(b) Exergy efficiency

(c) Total cost rate

Fig. 5.5: Effect of AC pressure ratio on the overall performance of CCHP systems.

the lower limit is set at 6. [20]. As per Fig. 5.5(a), η_{tot} of CCHP systems improves with the increase in r_p. According to Eq. (5.31), η_{tot} is the ratio of net energy output to the net energy supplied. Since $\dot{m}_f$ is kept constant, the energy supplied to all four CCHP systems is fixed. The energy output, which is the sum of the power, heating, and cooling generated from the entire CCHP system, does increase, when the AC pressure ratio rises, leading to a gain in energy efficiency. Similarly, as shown in Fig. 5.5(b), the exergy efficiency of all four CCHP systems increases with the increase in r_p. As per Eq. (5.32), ε_{tot} is the ratio of net exergy output to the net exergy supplied. The exergy delivered to all four CCHP systems is fixed because $\dot{m}_f$ is maintained fixed. The exergy output, which is the sum of the power, equivalent exergy of heating, and equivalent exergy of cooling generated by the overall CCHP system, does rise when r_p rises, increasing ε_{tot}. On the other hand,

as depicted in Fig. 5.5(c), $\dot{C}_{tot}$ of the CCHP systems increases with the increase in r_p. This is mainly because as r_p rises; the purchase equipment cost of AC increases dramatically, increasing the $\dot{Z}_{AC}$. It is justified because, as Eq. (5.4) illustrates, the purchasing equipment cost of the AC is directly proportional to r_p. Moreover, it is also observed that with the increase in r_p, the $\dot{C}_D$ of AC increases. It is because the irreversibility due to the impingement of air at the compressor blades increases with the rise in compressor outlet pressure.

AC isentropic efficiency

The efficiency with which electrical energy is transformed into the potential energy of compressed air in an air compressor is measured by $\eta_{s,AC}$. The divergence between the isentropic compression process and the real compression process decreases as $\eta_{s,AC}$ increases, resulting in a decrease in AC power consumption. This in turn increases the net power obtained from the GT cycle. Furthermore, the flue gas temperature (T_6) at the inlet of the HRSG is found to decrease with the increase in $\eta_{s,AC}$. It decreases the amount of heat recovered at the HRSG, which lowers $\dot{m}_s$ and subsequently decreases the power output of ST and RR-ORC. It is also observed that the cooling output of the ACS-I in system-I and system-IV decreases with the increase in $\eta_{s,AC}$. It is because the wet steam extracted from the ST is used as a heat source to drive the ACS-I in both system-I and system-IV, and when $\dot{m}_s$ drops, the cooling output obtained from the ACS-I likewise decreases. On the other hand, as $\eta_{s,AC}$ rises, the cooling output of the ACS-II in all four CCHP systems increases due to the increase in flue gas temperature (T_7) at the inlet of ACS-II's generator. In fact, it is observed that all CCHP systems produce more net energy as AC isentropic efficiency rises.

The impact of change in $\eta_{s,AC}$ on η_{tot}, ε_{tot}, and $\dot{C}_{tot}$ of the four CCHP systems are depicted in Figs. 5.6(a) to 5.6(c), respectively. The upper limit of $\eta_{s,AC}$ is set at 89%, while the lower limit is set at 80% [20]. Fig. 5.6(a) shows that η_{tot} of CCHP systems improves with the increase in $\eta_{s,AC}$. The reason for the increase in η_{tot} of all four systems is the increase in net energy output. Similarly, as shown in Fig. 5.6(b), ε_{tot} of all four CCHP systems increases with the increase in $\eta_{s,AC}$ owing to an increase in exergy outputs. On the other hand, as depicted in Fig. 5.6(c), the total cost rate of the CCHP systems increases with the increase in the AC's isentropic efficiency. It is also worth noting that the rate of increase of $\dot{C}_{tot}$ is low at lower $\eta_{s,AC}$, whereas the rate of increase of $\dot{C}_{tot}$ grows dramatically at higher $\eta_{s,AC}$. The increase in the purchasing equipment cost of the AC is the cause of the increase

in $\dot{C}_{tot}$ of the systems. However, it is observed that as $\eta_{s,AC}$ increases, $\dot{C}_D$ reduces due to the decrease in irreversibility present at the AC. Further, justification for the exponential rise of $\dot{C}_{tot}$ at higher $\eta_{s,AC}$ can be found in Eq. (5.4), which makes it abundantly evident that when $\eta_{s,AC}$ approaches the value of 90%, the purchasing equipment cost of the AC is inevitably going to rise exponentially.

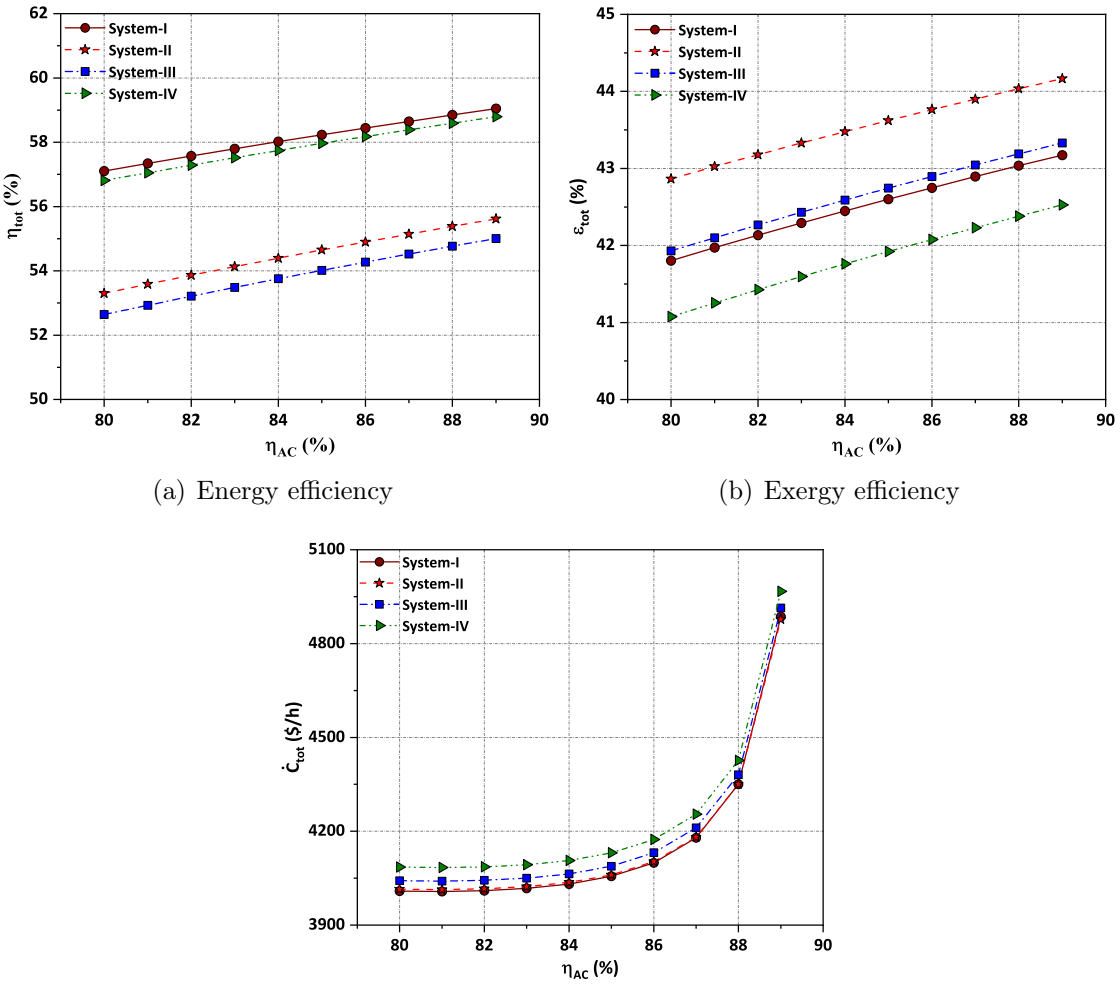

(a) Energy efficiency

(b) Exergy efficiency

(c) Total cost rate

Fig. 5.6: Effect of AC isentropic efficiency on the overall performance of CCHP systems.

GT isentropic efficiency

The efficiency with which the potential energy of combustion gas is converted into electrical energy in a gas turbine is measured by $\eta_{s,GT}$. The divergence between the real expansion process and the ideal (isentropic) expansion process decreases as $\eta_{s,GT}$ rises, increasing GT power output. Therefore, when $\eta_{s,GT}$ rises, more power is generated by the GT, increasing the net power obtained from the GT cycle.

Furthermore, it is revealed that as $\eta_{s,GT}$ increases, the flue gas temperature (T_6) at the HRSG's inlet decreases. Correspondingly, the amount of heat recovered at the HRSG also decreases which indeed reduces $\dot{m}_s$ and hence the net power obtained from the ST and RR-ORC is also reduced. The cooling output of the ACS-I in system-I and system-IV is also seen to decrease with the rise in $\eta_{s,GT}$. It is because the wet steam extracted from the ST is employed as a heat source to drive the ACS-I in both system-I and system-IV, and as $\dot{m}_s$ decreases, so do the cooling output received from the ACS-I. On the contrary, the cooling output of the ACS-II in all four CCHP systems increases with the rise in $\eta_{s,GT}$. The reason for the increase in ACS-II's cooling output is the rise in flue gas temperature (T_7) at the inlet of ACS-II's generator. In general, it is observed that all CCHP systems produce more net energy output as $\eta_{s,GT}$ rises.

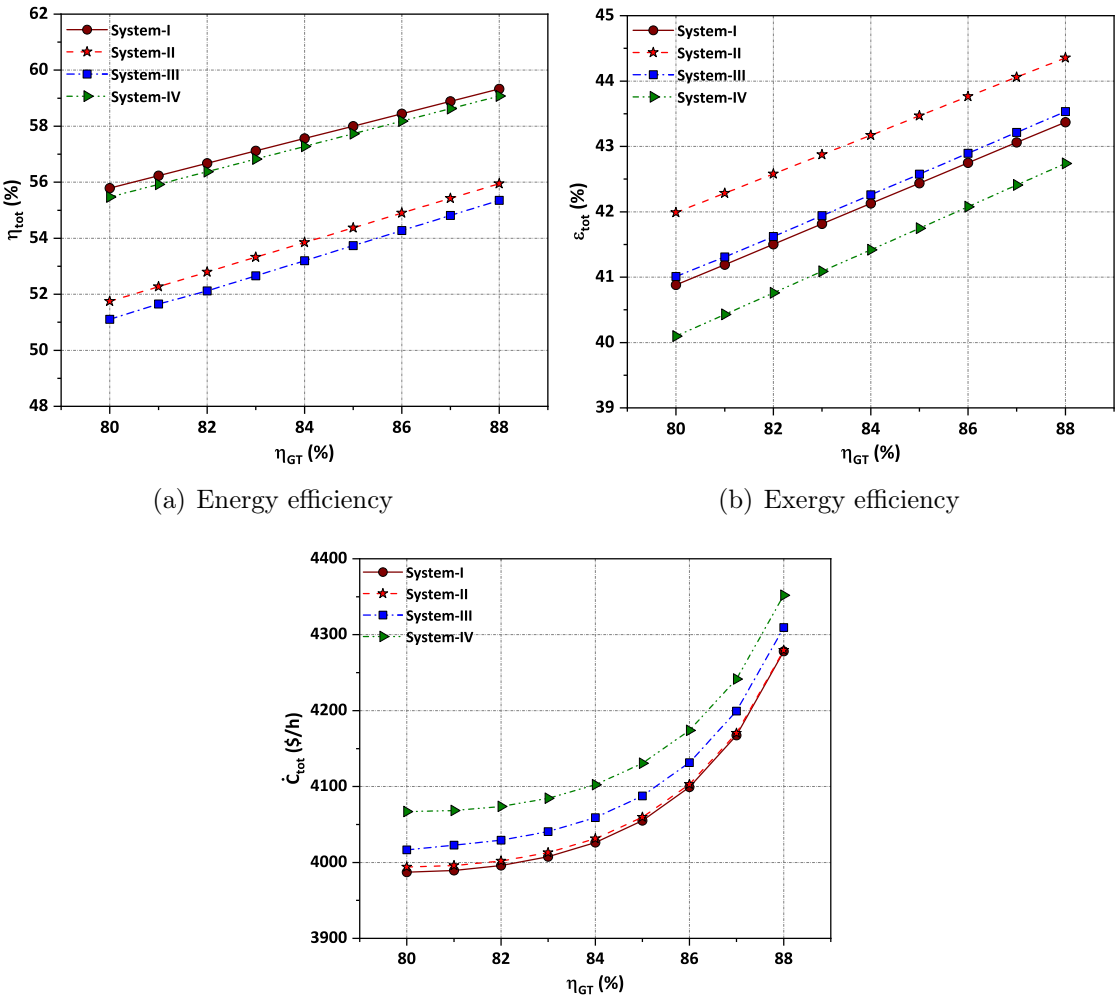

(a) Energy efficiency

(b) Exergy efficiency

(c) Total cost rate

Fig. 5.7: Effect of GT isentropic efficiency on the overall performance of CCHP systems.

The effect of change in $\eta_{s,GT}$ on η_{tot}, ε_{tot}, and $\dot{C}_{tot}$ of the four CCHP systems are depicted in Figs. 5.7(a) to 5.7(c), respectively. The upper limit of $\eta_{s,GT}$ is set at 88%, while the lower limit is set at 80% [20]. Fig. 5.7(a) shows that with the increase in $\eta_{s,GT}$, η_{tot} of the CCHP systems increases linearly. It is because as $\eta_{s,GT}$ increases, the net energy obtained from the CCHP systems increases. Likewise, as shown in Fig. 5.7(b), ε_{tot} of all four CCHP systems increases with the increase in $\eta_{s,GT}$ due to the increase in net product exergy. Fig. 5.7(c) shows that as $\eta_{s,GT}$ increases, $\dot{C}_{tot}$ of the CCHP systems increases. Additionally, it is noteworthy that at lower $\eta_{s,GT}$, the rate of increase of $\dot{C}_{tot}$ is modest, whereas, at higher $\eta_{s,GT}$, the rate of increase of $\dot{C}_{tot}$ increases considerably. The increase in the purchasing equipment cost of the GT is the cause of the increase in $\dot{C}_{tot}$ of the systems. The $\dot{C}_D$ does, however, appear to decrease as $\eta_{s,GT}$ rises as a result of the reduced irreversibility at the GT. Additionally, Eq. (5.6) provides support for the exponential growth of $\dot{C}_{tot}$ at increasing $\eta_{s,GT}$, making it clear that when the $\eta_{s,GT}$ approaches near to 92%, the purchasing equipment cost of the GT inevitably increases exponentially.

APH outlet temperature

The rise in APH output temperature (T_3) signifies an increase in the temperature of compressed air entering the CC. It is found that when T_3 rises, the temperature of the combustion gas (T_4) entering the GT also rises, increasing the extent of expansion and, subsequently, increasing the net GT power. Furthermore, it is revealed that as T_3 increases, the flue gas temperature (T_6) at the HRSG's inlet decreases modestly. Correspondingly, the amount of heat recovered at the HRSG also decreases which indeed reduces $\dot{m}_s$ and hence the net power obtained from the ST and the RR-ORC is also reduced. Moreover, the cooling output of the ACS-I in system-I and system-IV is also seen to decrease marginally with the rise in T_3 due to the decrease in the mass flow rate of wet steam extracted from the ST. On the contrary, the cooling output of the ACS-II in all four CCHP systems increases slightly with the rise in T_3. The reason for the increase in ACS-II's cooling output is the marginal rise in flue gas temperature (T_7) at the inlet of ACS-II's generator. In general, it is seen that as T_3 rises, the net energy output from all CCHP systems also increases.

The effect of change in T_3 on η_{tot}, ε_{tot}, and $\dot{C}_{tot}$ of the four CCHP systems are depicted in Figs. 5.8(a) to 5.8(c), respectively. The upper limit of T_3 is set at 810 K, while the lower limit is set at 750 K [20]. Fig. 5.8(a) depicts that η_{tot} of the CCHP systems slightly improves when T_3 rises. It is because the net energy obtained from the CCHP systems rises with the increase in T_3. Similarly, as shown in Fig. 5.8(b),

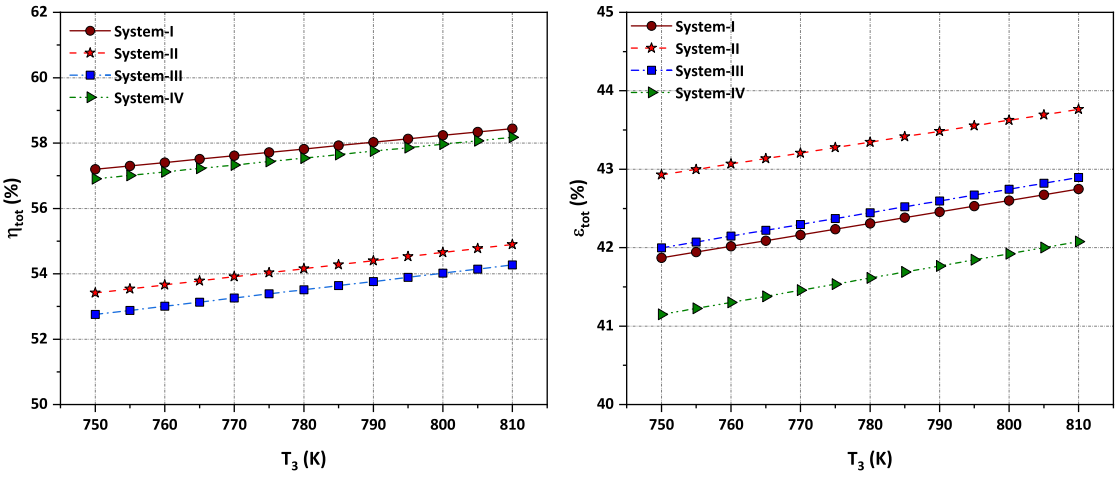

(a) Energy efficiency

(b) Exergy efficiency

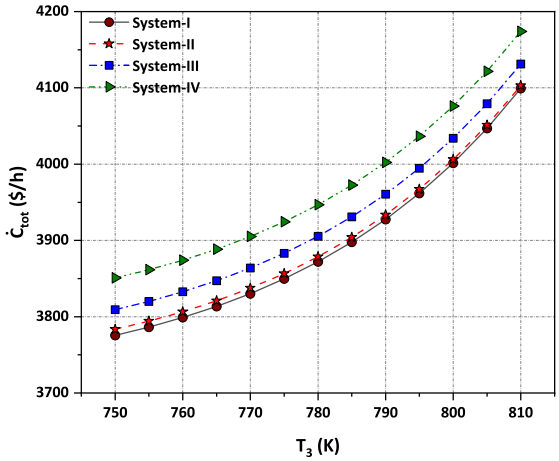

(c) Total cost rate

Fig. 5.8: Effect of APH outlet temperature on the overall performance of CCHP systems.

ε_{tot} of all four CCHP systems increases with the increase in T_3 due to the increase in net product exergy. Moreover, $\dot{C}_{tot}$ of the CCHP systems also increases with the rise in T_3, as per Fig. 5.8(c). It is particularly due to the increase in $\dot{C}_D$ and $\dot{Z}_k$ of the APH. The $\dot{C}_D$ rises as irreversibility due to an increase in heat loss from the APH to the ambient rises. In addition, $\dot{Z}_k$ of the APH increased due to the increase in LMDT across the APH.

ST inlet pressure

The upper limit considered for the pressure at state 12 (P_{12}) in system-I and system-II is 19500 kPa while that in system-III and system-IV are 11500 kPa and 12000 kPa, respectively. The criterion employed in this study to determine the maximum

limit of the ST inlet pressure is that the quality of steam exiting the ST does not fall below 88% [23]. It is because if the moisture content of steam at the later stages of ST is high, the life of turbine blades reduces due to erosion. Additionally, 8000 kPa is taken into account as the minimum ST inlet pressure for carrying out the parametric study. It is observed that as ST inlet pressure increases, the power obtained from the ST cycle for all four CCHP systems increases due to the increase in the average temperature of heat addition [9, 23]. However, as compared to system-I and system-II, the increase in ST power is marginal in system-III and system-IV. It is because the upper limit of ST inlet pressure in both system-III and system-IV is comparatively lower than that of system-I and system-II. Moreover, $\dot{m}_s$ first reduces and then increases with an increase in ST inlet pressure. As a result, the magnitude of supplied heat by the wet steam at the generator of the RR-ORC also first reduces and then increases. Therefore, the RR-ORC's power modestly decreases first and again marginal increases in system-I and system-II. In fact, for the same reason, the cooling output of the ACS-I in system-I and system-IV is also observed to slightly decrease at first then again increase marginally. On the contrary, it is observed that the cooling output of the ACS-II in system-I and system-II increases first and then again decreases. It is because as $\dot{m}_s$ decreases the temperature of the flue gas at the inlet of the ACS-II's generator increases. On the other hand, the temperature of the flue gas at the inlet of the ACS-II's generator decreases as $\dot{m}_s$ increases at greater ST inlet pressure. It is also observed that the cooling output of the ACS-II in system-III and system-IV increases linearly. System-III and System-IV do not exhibit the increasing-decreasing trend of ACS-cooling II's output since ST inlet pressure could not be raised to a higher level in both systems due to steam quality restrictions.

The effect of change in ST inlet pressure on η_{tot}, ε_{tot}, and $\dot{C}_{tot}$ of the four CCHP systems are depicted in Figs. 5.9(a) to 5.9(c), respectively. Fig. 5.9(a) shows that η_{tot} of the CCHP systems improves when the P_{12} rises. It is because the net energy obtained from the CCHP systems rises with the increase in P_{12}. Similarly, as shown in Fig. 5.9(b), ε_{tot} of all four CCHP systems increases with the increase in P_{12} due to the increase in net product exergy. Moreover, $\dot{C}_{tot}$ of system-I and system-II decreases with the rise in P_{12}, as per Fig. 5.9(c). However, it has been found that at lower P_{12}, the rate of decrease of $\dot{C}_{tot}$ is low, while at higher P_{12}, the rate of decrease of $\dot{C}_{tot}$ is significant. It is because, even while the purchase equipment costs of ST and HRSG rise, the purchase equipment costs of RR-ORC and ACS-II components decrease, and the rate of reduction is larger at higher P_{12}. Further, $\dot{C}_{tot}$ of system-

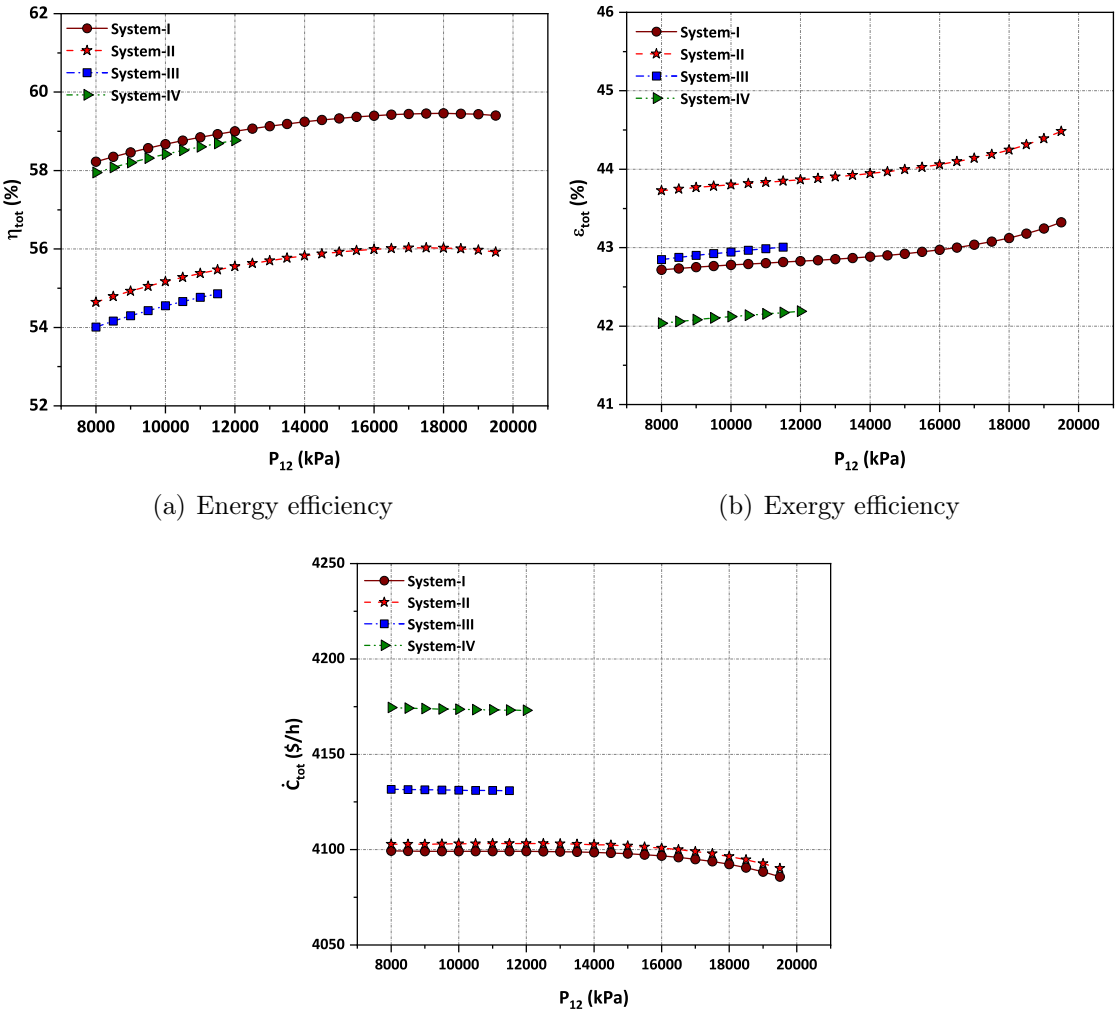

(a) Energy efficiency

(b) Exergy efficiency

(c) Total cost rate

Fig. 5.9: Effect of ST inlet pressure on the overall performance of CCHP systems.

III and system-IV decreases marginally with the rise in P_{12}, as per Fig. 5.9(c). For system-III and system-IV, a significant drop in $\dot{C}_{tot}$ is not observed because P_{12} could not be raised to a higher level in both systems due to steam quality restrictions.

PPTD

The upper limit of $\Delta T_{pp,HRSG}$ is set at 50 K, while the lower limit is set at 20 K [19]. It is observed that as $\Delta T_{pp,HRSG}$ increases, the power obtained from the ST cycle for all four CCHP systems decreases. The increase in $\Delta T_{pp,HRSG}$ denotes an increase in the difference between the temperature of flue gas entering the evaporator and the saturation temperature of the water. In fact, the water's saturation temperature remains unchanged until P_{12} is fixed. It reveals that the HRSG's capacity to recover heat from flue gas is declining as the temperature of the flue gas entering the evap-

orator section rises. As a result, $\dot{m}_s$ decreases, which decreases the power produced by the ST cycle. Moreover, due to the decrease in $\dot{m}_s$, the amount of heat delivered by the wet steam at the generator of the RR-ORC also reduces. Therefore, the RR-ORC's power modestly decreases in system-I and system-II with the increase of ST inlet pressure. Likewise, the cooling output of the ACS-I in system-I and system-IV is also reduced. It is due to the decrease in the amount of waste heat supplied to the generator of the ACS-I owing to the decrease in the mass flow rate of wet steam extracted from the ST. On the contrary, it is observed that the cooling output of the ACS-II in all four systems increases linearly with the increase in $\Delta T_{pp,HRSG}$. It is because the heat recovered from the flue gas at the generator of ACS-II increases due to the decrease in the heat recovery at the HRSG.

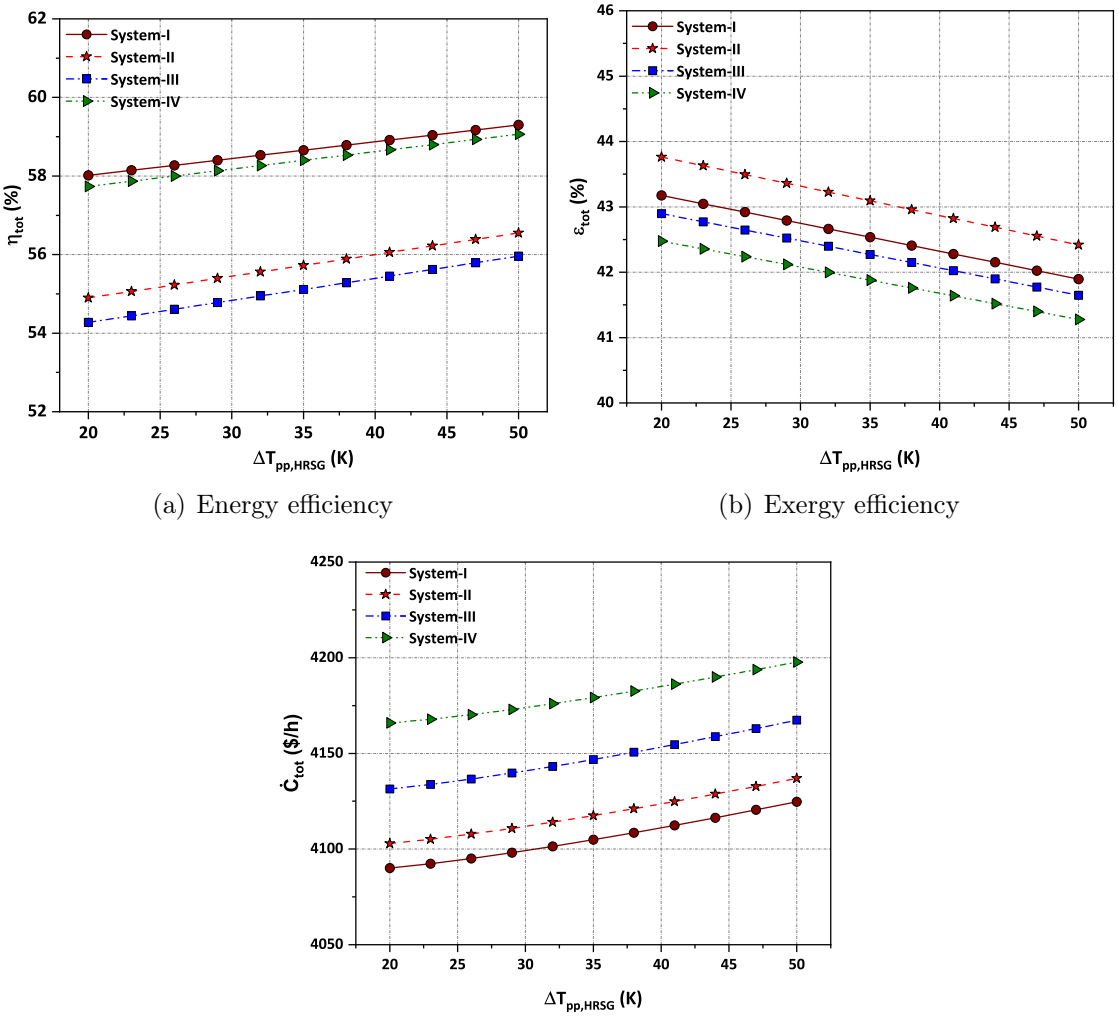

(a) Energy efficiency

(b) Exergy efficiency

(c) Total cost rate

Fig. 5.10: Effect of PPTD on the overall performance of CCHP systems.

The effect of change in $\Delta T_{pp,HRSG}$ on η_{tot}, ε_{tot}, and $\dot{C}_{tot}$ of the four CCHP systems

are depicted in Figs. 5.10(a) to 5.10(c), respectively. Fig. 5.10(a) shows that η_{tot} of the CCHP systems improves when the rise in $\Delta T_{pp,HRSG}$. The reason for the increase in η_{tot} is the increase in net energy output obtained from the systems. Although the power obtained from the ST cycle and RR-ORC decreases with an increase in η_{tot}, the cooling output of the ACS-II increases dramatically, leading to an increase in net energy output. Furthermore, the product exergy is equal to the power, but it only accounts for a minor portion of the cooling or heating output. As a result, the net product exergy of the systems decreases with the increase in $\Delta T_{pp,HRSG}$. Consequently, as seen in Fig. 5.10(b), ε_{tot} of the CCHP systems similarly declines as $\Delta T_{pp,HRSG}$ rises. Furthermore, it can be seen from Fig. 5.10(c) that $\dot{C}_{tot}$ of systems rises with the increase in $\Delta T_{pp,HRSG}$. It is because as the $\Delta T_{pp,HRSG}$ increases, the purchase equipment cost of the HRSG increases significantly due to the increase in the heat transfer area [15, 19]. Although the cost of exergy destruction of the HRSG falls as $\Delta T_{pp,HRSG}$ rises, the purchase equipment cost of the HRSG increases more significantly, increasing $\dot{C}_{tot}$ of the CCHP systems. The increase in purchase equipment cost of the ACS-II also contributes to the rise in $\dot{C}_{tot}$ of the CCHP systems.

The parametric analysis showed that, for all the operating conditions taken into consideration, trade-offs exist between the objective functions. It is important to note that among the objective functions, an improvement in η_{tot} and ε_{tot} is desirable, whereas an increase in $\dot{C}_{tot}$ is undesirable. The parametric results revealed that as r_p, $\eta_{s,AC}$, $\eta_{s,GT}$, and T_3 increases, η_{tot} and ε_{tot} also increases, but at the same time, $\dot{C}_{tot}$ rises too. In the meantime, as P_{12} rises, η_{tot} and ε_{tot} rises and $\dot{C}_{tot}$ falls, but at higher P_{12}, η_{tot} begins to decline modestly. Lastly, as $\Delta T_{pp,HRSG}$ rises, η_{tot} and $\dot{C}_{tot}$ increase whereas the ε_{tot} reduces. Therefore, multi-objective optimization is required to obtain the optimal operating conditions for the CCHP systems. Since parametric analysis cannot give direct favourable operating conditions for the CCHP systems due to the presence of trade-offs.

5.3.5 Multi-objective optimization-based results

The PESA-II is stochastic as it initiates with randomly generated solutions. This gives a slight deviation in results with every execution. Therefore, in this study, the robustness and reproducibility of the algorithm are assessed by executing the PESA-II routine for 30 runs. Thereafter, the coefficient of variation, which is the ratio of standard deviation and mean, is calculated for each of the decision variables for all four systems. It was observed that the coefficient of variation for each decision

variable in all four systems is less than 5% [21]. It suggests that the solutions obtained from the optimization processes are reliable. Moreover, the optimization results obtained from the 15th run for each system are presented here.

The 3D Pareto front generated from the multi-objective optimization of system-I using energy efficiency, exergy efficiency, and total cost rate as the objective functions is shown in Fig. 5.11(a). The 3D Pareto front is projected in an objective space with energy efficiency on the x-axis, exergy efficiency on the y-axis, and total cost rate on the z-axis. As previously established, the purpose of this research is to maximize energy and exergy efficiency while lowering the total cost rate of both CCHP systems. In this study, the 3D Pareto front is also presented from multiple perspectives for greater interpretation. Fig. 5.11(b) presents the top view of the 3D Pareto front with energy efficiency on the x-axis and exergy efficiency on the y-axis. Similarly, Figs. 5.11(c) to 5.11(d) show the front and side views of the 3D Pareto front, respectively. Fig. 5.11(c) is projected in a 2D objective space with energy efficiency on the x-axis and total cost rate on the y-axis. On the other hand, Fig. 5.11(d) is projected in a 2D objective space with exergy efficiency on the x-axis and total cost rate on the y-axis. The broad inference from Fig. 5.11(b) is that energy and exergy efficiency do not have a significant trade-off. It is because, for a large number of optimal solutions, a greater value of energy efficiency corresponds to a larger value of exergy efficiency, which is desirable. Figs. 5.11(c) to 5.11(d), on the other hand, illustrates that energy efficiency and exergy efficiency have a conflicting relation with the total cost rate. It is because, for a large number of optimal solutions, a higher value of energy and exergy efficiency corresponds to a higher value of total cost rate, which is undesirable. Likewise, the 3D Pareto front and its corresponding top, front and side views for system-II to system-IV are shown in Figs. 5.12 to 5.14, respectively. The Pareto fronts of system-II, system-III, and system-IV exhibit the same pattern as system-I, as shown in Figs. 5.12 to 5.14. For the majority of optimal solutions, a higher value of energy efficiency equates to a higher value of exergy efficiency, which indicates there is no considerable conflict between energy and exergy efficiency. On the other hand, a greater value of energy and exergy efficiency correlates to a higher value of the total cost rate for a large number of optimal solutions, which indicates there is considerable conflict between both energy and exergy efficiency with the total cost rate.

The best optimal solutions selected by using the Entropy-TOPSIS method from the Pareto fronts corresponding to system-I to system-IV are also highlighted in Figs. 5.11 to 5.14, respectively. The weights evaluated by using the Entropy method

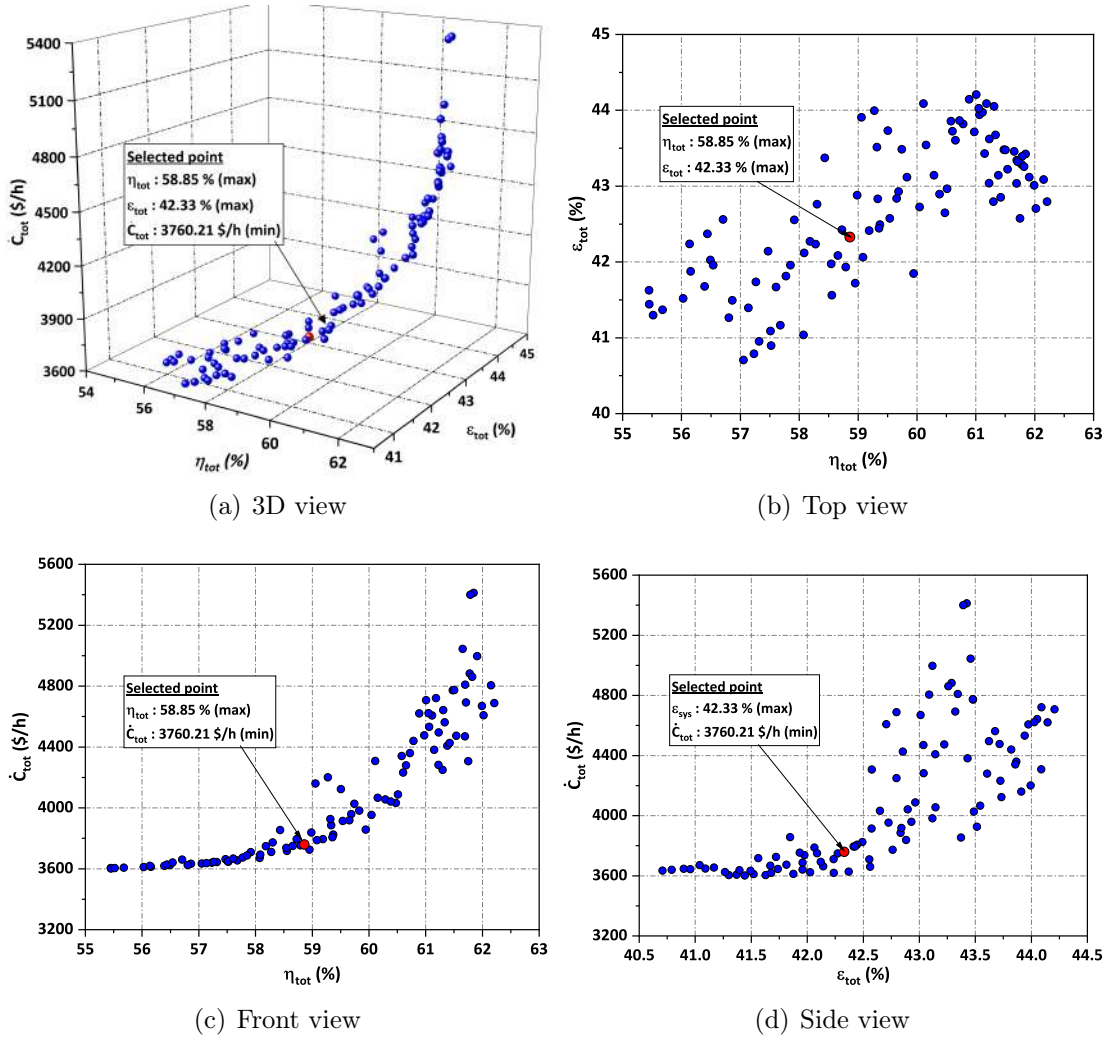

(a) 3D view (b) Top view

(c) Front view (d) Side view

Fig. 5.11: Pareto front obtained from the multi-objective optimization of system-I.

from the Pareto fronts of all the CCHP systems are shown in Table 5.23. These weights are subsequently assigned to the TOPSIS decision-maker for determining the best optimal solutions from the set of optimal solutions obtained through multi-objective optimization. As seen in Table 5.23, the weights for energy efficiency, exergy efficiency, and total cost rate are denoted as w_1, w_2, and w_3, respectively. It is also observed that as per the algorithm of TOPSIS, the summation of all the weights is unity. It can also be seen that the values of weights for all three objective functions are almost the same which implies that the objective functions are given almost equal priority.

The values of the optimal decision variables corresponding to the best optimal solution for all four CCHP systems are shown in Table 5.24. Each of the decision variables has unique values that fall within the given upper and lower bounds. Additionally, Table 5.25 provides the values of the objective functions corresponding

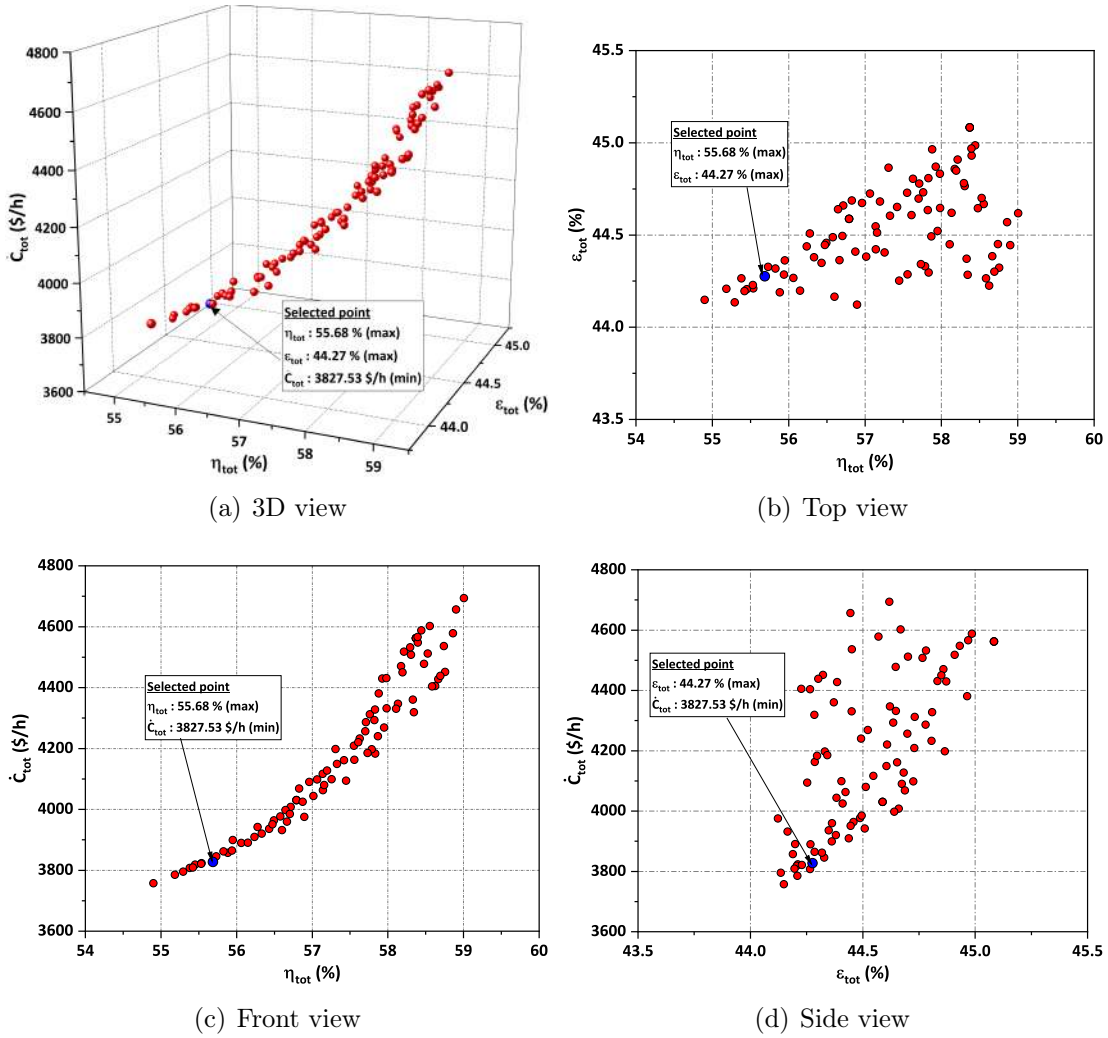

(a) 3D view (b) Top view

(c) Front view (d) Side view

Fig. 5.12: Pareto front obtained from the multi-objective optimization of system-II.

Table 5.23: The weights of each objective function estimated using the Entropy method.

CCHP Systems	w_1	w_2	w_3
System-I	0.3341	0.3342	0.3317
System-II	0.3337	0.3338	0.3325
System-III	0.3336	0.3338	0.3326
System-IV	0.3337	0.3337	0.3326

to the four CCHP systems with regard to the optimal decision variables and base case condition. As can be observed, at the optimal state, the energy and exergy efficiencies of system-I are 58.85% and 42.33%, respectively, with a total cost rate of 3760.21 $/h. The energy and exergy efficiencies of system-II, however, are 55.68% and 44.27%, respectively, and the total cost rate is 3827.53 $/h. System-III has energy and exergy efficiencies of 55.01% and 41.92%, respectively, with a total cost rate

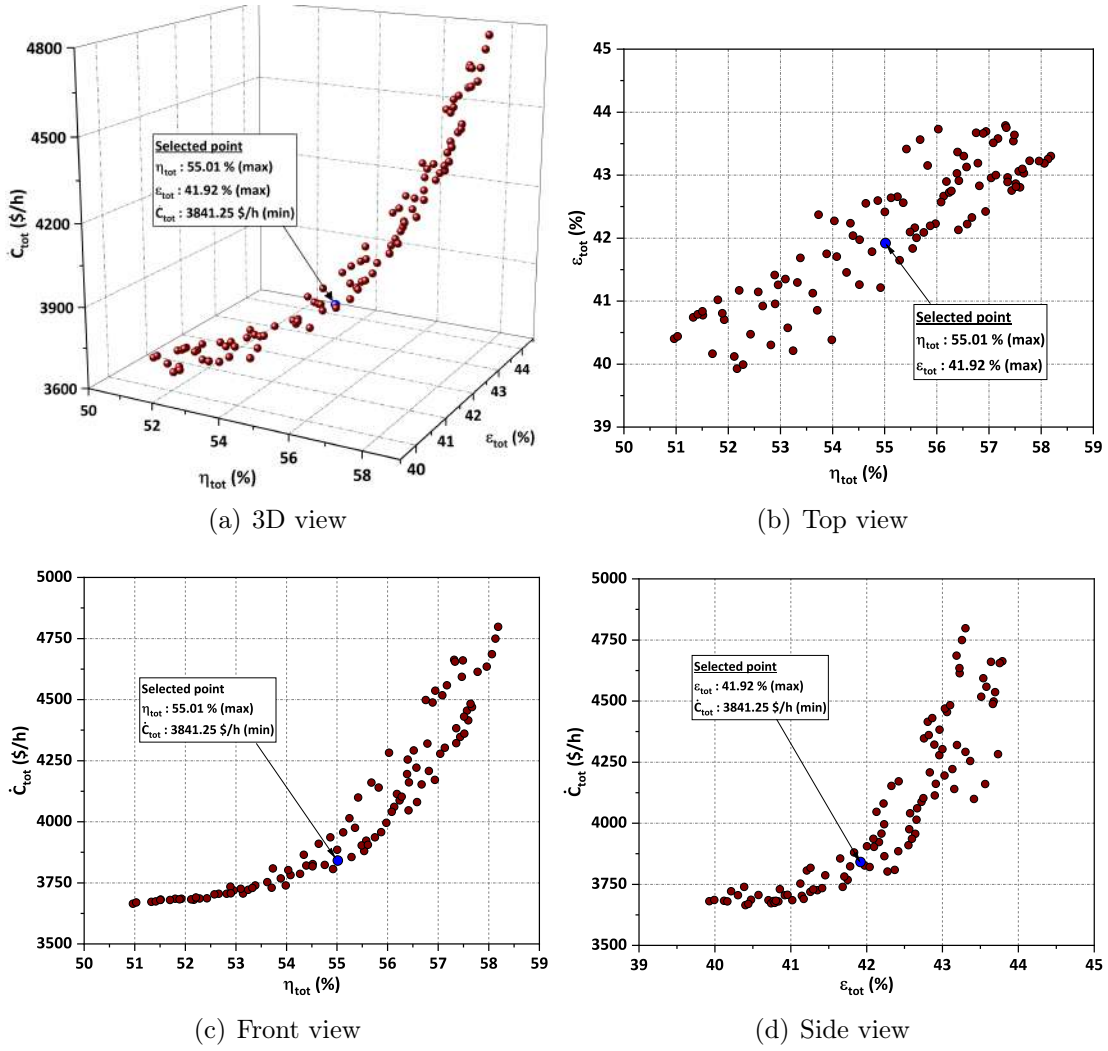

(a) 3D view

(b) Top view

(c) Front view

(d) Side view

Fig. 5.13: Pareto front obtained from the multi-objective optimization of system-III.

of 3841.25 $/h. System-IV, on the other hand, has energy and exergy efficiencies of 58.00% and 41.59%, respectively, with a total cost rate of 3851.60 $/h. Table 5.25 further shows that post optimization, the energy and exergy efficiency of all four CCHP systems improved while the total cost rate decreased. The increase in energy efficiency is highest for system-III, with a 3.19% improvement, while the increase in exergy efficiency is highest for system-II, with a 4.21% increment. Moreover, the decrease in total cost rate is highest for system-I with a decrement of 1.45%. Based on the comparison, it can be inferred that the overall performance of the CCHP systems is improved after performing the multi-objective optimization. Now to compare the performance of the CCHP systems based on the results obtained at the optimal state, the usage of multi-criteria decision approaches is necessary. It is because no single system can be considered the best system. After all, system-I has the highest energy efficiency and the lowest total cost rate, but system-II has

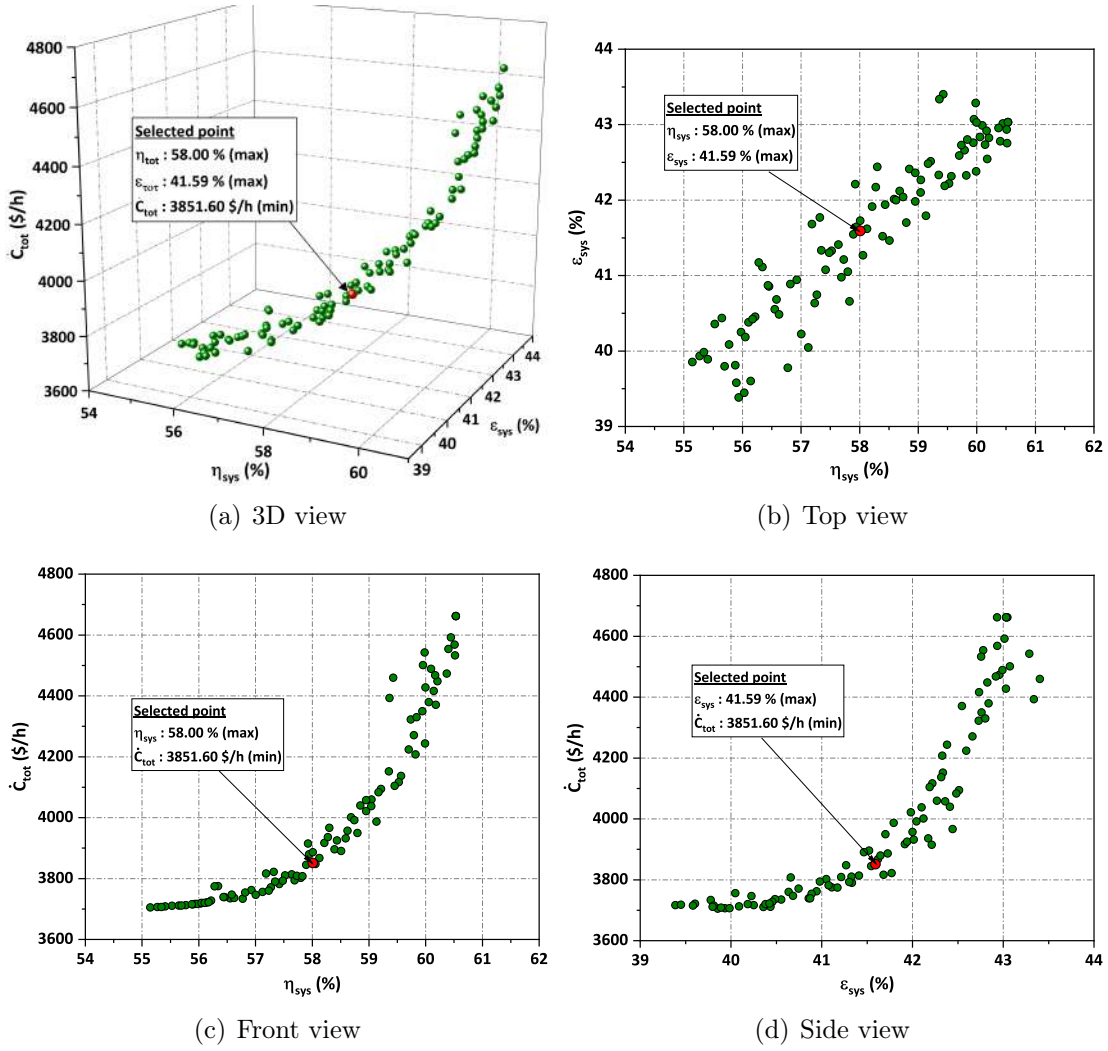

(a) 3D view (b) Top view

(c) Front view (d) Side view

Fig. 5.14: Pareto front obtained from the multi-objective optimization of system-IV.

the highest exergy efficiency. The best-performing CCHP system among the four systems should ideally be the one with the highest energy and energy efficiency and the lowest total cost rate. Therefore, the Entropy-TOPSIS decision-maker is once again employed at this stage to select the best-performing CCHP system. Table 5.25 is turned into a multi-criteria decision-making problem by considering the objective functions as the criterion and the CCHP systems as an alternative (refer to Chapter 4 (Section 4.2.5)). The weights evaluated for energy efficiency, exergy efficiency and total cost rate are 0.5341, 0.4059 and 0.060, respectively. Based on the calculated weights, the TOPSIS decision-maker ranked system-I as the best-performing CCHP system. The system-IV is found to be the second-best performing system, while system-II and system-III are the third and fourth-best CCHP systems, respectively.

To observe the variations of the decision variables, the scattered distribution plots of the decision variables corresponding to all four CCHP systems are provided

in Figs. 5.15(a) to 5.15(f). The scattered distribution plots illustrate the distribution of the non-dominated population in the decision space. It shows how a decision variable affects the trade-offs that exist between the objective functions. The upper and lower limits of the decision variables are also shown in the scattered plots with dotted lines. Fig. 5.15(a) shows the scattered distribution plot of the AC pressure ratio. As can be seen, the population corresponding to the AC pressure ratio for all four CCHP systems is explicitly distributed over a large decision space. It implies that the AC pressure ratio is one of the sources of trade-offs among the objective functions in all four systems. Similarly, the population corresponding to the AC isentropic efficiency for each of the four CCHP systems is distributed over a large decision space (refer to Fig. 5.15(b)). It implies that isentropic efficiency also contributes to the conflicting nature of the objective functions in all four systems. Additionally, the majority of the candidate solutions are dispersed, within a range of 82 to 88%.

Table 5.24: The optimal values of the decision variables.

Parameters	Units	System-I	System-II	System-III	System-IV
r_p	–	10.02	10.59	10.22	10.89
$\eta_{s,AC}$	%	84.70	84.06	84.21	83.23
$\eta_{s,GT}$	%	87.37	87.54	87.62	87.63
T_3	K	755.95	754.75	764.52	760.05
P_{12}	kPa	17279.26	19389.74	11303.58	11581.62
$\Delta T_{pp,HRSG}$	K	35.75	20.08	35.46	31.69

Table 5.25: Comparison of objective function values at the base case and optimal conditions.

Systems	η_{tot} (%)			ε_{tot} (%)			$\dot{C}_{tot}$ (\$/h)		
	Base	Optimal	Δ (%)	Base	Optimal	Δ (%)	Base	Optimal	Δ(%)
System-I	57.20	58.85	+2.88	41.87	42.33	+1.09	3815.4	3760	-1.45
System-II	53.96	55.68	+3.18	42.48	44.27	+4.21	3830.4	3827.53	-0.07
System-III	53.31	55.01	+3.19	41.58	41.92	+0.82	3856.7	3841.25	-0.40
System-IV	56.90	58.00	+1.93	41.14	41.59	+1.09	3890.8	3851.60	-1.02

The scattered distribution plot for the GT isentropic efficiency is depicted in Fig. 5.15(c). It demonstrates that the population is primarily distributed near the upper limit (86-88%) for all four systems. It suggests that with a higher GT isentropic efficiency, the improvement in energy and exergy efficiency outweighs the increase in total cost rate. It is justified because the parametric analysis (see Fig. 5.7) revealed that when the GT isentropic efficiency was increased, the improvement in

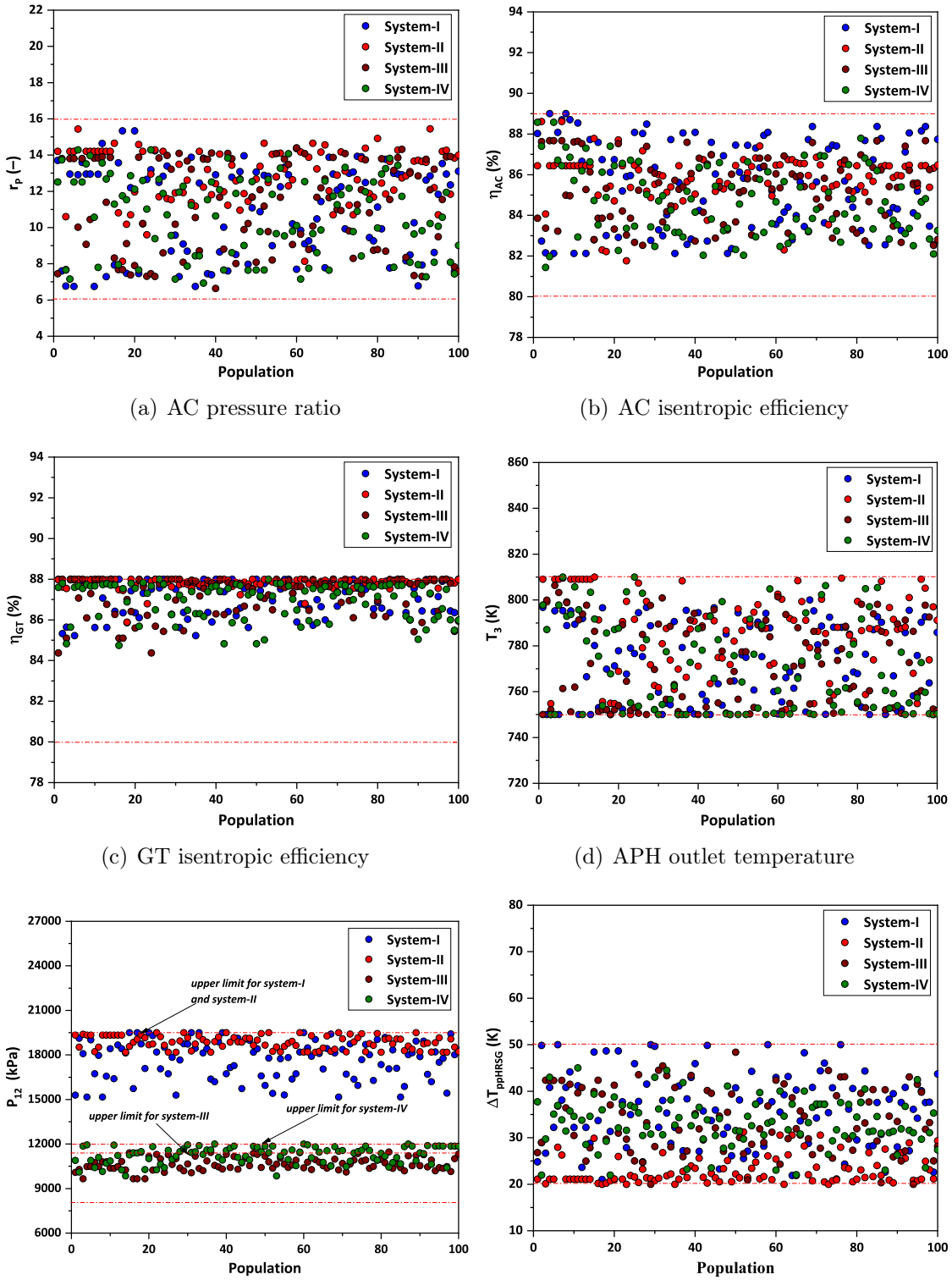

(a) AC pressure ratio

(b) AC isentropic efficiency

(c) GT isentropic efficiency

(d) APH outlet temperature

(e) ST inlet pressure

(f) PPTD

Fig. 5.15: Scattered distribution plots of decision variables.

energy and exergy efficiency was linear, whereas the increase in total cost rate was parabolic with exponential rise near the upper limit. However, the increase in en-

ergy and exergy efficiency was likewise linear in the case of AC isentropic efficiency (see Fig. 5.6), and the increase in total cost rate was parabolic with an exponential rise near the upper limit. The population of AC isentropic efficiency, however, is not dispersed towards the upper limit because the exponential rise in AC isentropic efficiency is greater than that of GT isentropic efficiency. Fig. 5.15(d) shows the scattered distribution plot for the APH outlet temperature. As can be seen, though the population is scattered over the entire region of the decision space, most of the candidate solutions are near the lower limit. It demonstrates that the optimal operating range for the APH outlet temperature is between 750 K and 770 K.

The scattered distribution plot for ST inlet pressure is shown in Fig. 5.15(e). The scattered distribution plot shows that, while all four CCHP systems have the same lower limit, the upper limit of system-I and system-II is 19500 kPa and that of system-III and system-IV are 11500 kPa and 12000 kPa, respectively. It can be seen that for system-I, the population is randomly distributed over the range of 15000 kPa to 19500 kPa in the decision space, with the majority being concentrated at the upper limit (19500 kPa). It suggests that for system-I, the ST inlet pressure has a small impact on the trade-off solution. It is noted that almost all of the candidate solutions for system-II are present near the upper limit (19500 kPa). It indicates that for system-II, ST inlet pressure does not contribute significantly towards the trade-off solution. This indicates that the ST inlet pressure near 19500 kPa provides higher energy and exergy efficiency and lower total cost rates. Similarly, the population for system-III and system-IV are randomly distributed in a confined decision space at their respective upper bounds. It indicates that the ST inlet pressure also has a minimal impact on the trade-off solution for system-III and system-IV. Lastly, the scattered distribution plot for PPTD is shown in Fig. 5.15(f). The scattered distribution plot shows that for all four CCHP systems, the population is randomly distributed over the decision space, with the majority being concentrated near the lower limit. It shows that PPTD does contribute significantly to the trade-off solution and it is preferable to keep PPTD close to the lower limit.

5.4 Summary

In this chapter, four configurations of GT-based combined cooling, heating and power (CCHP) systems are proposed. In these systems, the exhaust heat of a topping recuperative GT plant is utilized for further power, cooling and heating generation. Steam turbines and recuperative-regenerative organic Rankine cycles are used for

power generation by integrating those in a completely different arrangement. The absorption cooling systems are driven respectively by steam and exhaust heat for the generation of cooling load. The performances of the proposed systems are evaluated using energy, exergy, exergoeconomic and environmental (4E) analysis. Then the performance of the CCHP systems is also compared with the already discussed CPC systems under identical operating conditions. Thereafter, the behaviour of critical decision variables is studied by undertaking a parametric analysis. Then the CCHP systems are optimized considering energy efficiency, exergy efficiency and total cost rate as the objective functions using PESA-II. Further, the best optimal solutions are determined for all four CCHP systems from the Pareto fronts using Entropy-TOPSIS decision-maker. The main findings obtained from this study are presented below:

- System-I gives the highest net energy output of 72.48 MW where the power output is 55.52 MW, the heating output is 1.22 MW and the remaining 15.74 MW is the cooling output. System-I also has the highest energy efficiency of 57.85%, making it the most effective system among its counterparts.

- The CC has the highest irreversibility of all system components, with exergy destruction of 52.01 MW, accounting for more than 70% of the overall exergy destruction of the respective systems. The combustion reaction, heat transfer and fluid friction are the sources of irreversibilities in the CC. As a result, the cost due to exergy destruction is also the highest in the CC among all the components.

- The recuperative GT is the most efficient component in all four systems with the highest exergy efficiency of 95.10%. It implies that the GT could convert the fuel exergy fed to it into product exergy with the highest efficiency. In the topping GT plant, the CC has the least exergy efficiency of 70.84%. It is justified because the irreversibilities present in the CC cause most of the fuel's exergy to be destroyed, thus lowering the exergy efficiency.

- Among all the components, the capital investment cost rate for the AC in system-I and system-II is found to be the highest. However, among all the system-III and system-IV components, ST has the greatest capital investment cost.

- The exergoeconomic analysis showed that CC is the most crucial component with the highest $\dot{C}_D + \dot{Z}$ of 204.42 \$/h in all four systems. Moreover, the

majority of the cost associated with CC is due to exergy destruction. The AC is the second most critical component in system-I and system-II with the respective $\dot{C}_D + \dot{Z}$ values of 204.42 \$/h each. On the other hand, ST is the second most critical component in system-III and system-IV with the respective $\dot{C}_D + \dot{Z}$ values of 213.17 \$/h and 212.65 \$/h.

- The environmental cost rate for all four systems is found to be the same (477.27 \$/h). On the other hand, even though the rate of CO_2 emissions is the same for all four systems, system-I has the lowest (93.57 kg/MWh) specific CO_2 emission since it generates the highest net energy output. Moreover, the total cost rate for system-I is found to be the lowest among all the CCHP systems with 3815.4 \$/h.

- A comparative study between the configurations of CPC systems and CCHP systems at the same operating condition revealed that the CCHP systems perform far better with superior energy and exergy efficiency and lower total cost rates.

- Post optimization, the energy and exergy efficiency of all four CCHP systems improved while the total cost rate decreased. The increase in energy efficiency is highest for system-III, with a 3.19% improvement, while the increase in exergy efficiency is highest for system-II, with a 4.21% increment. Moreover, the decrease in total cost rate is highest for system-I with a decrement of 1.45%. Based on the comparison, it can be inferred that the overall performance of the CCHP systems is improved after performing the multi-objective optimization.

- Assessment of the scattered distribution plots revealed that the key variables that have the greatest impact on the trade-off solutions among the objective functions are the AC pressure ratio, AC isentropic efficiency, APH outlet temperature, and PPTD.

- Utilizing energy efficiency, exergy efficiency, and total cost rates as criteria, Entropy-TOPSIS decision-maker was used to rank the CCHP systems. The optimum conditions were used to evaluate each criterion for the four CCHP systems. It was found that system-I is the best-performing CCHP system.

Bibliography

[1] Ahmadi, P. *Modeling, analysis and optimization of integrated energy systems for multigeneration purposes*. PhD thesis, Faculty of Engineering and Applied Science, Ontario Tech University, 2013.

[2] Ahmadi, P. and Dincer, I. Thermodynamic and exergoenvironmental analyses, and multi-objective optimization of a gas turbine power plant. *Applied Thermal Engineering*, 31(14-15):2529–2540, 2011.

[3] Ahmadi, P., Dincer, I., and Rosen, M. A. Exergy, exergoeconomic and environmental analyses and evolutionary algorithm based multi-objective optimization of combined cycle power plants. *Energy*, 36(10):5886–5898, 2011.

[4] Ahmadi, P., Rosen, M. A., and Dincer, I. Greenhouse gas emission and exergo-environmental analyses of a trigeneration energy system. *International Journal of Greenhouse Gas Control*, 5(6):1540–1549, 2011.

[5] Alao, M. A., Ayodele, T. R., Ogunjuyigbe, A., and Popoola, O. Multi-criteria decision based waste to energy technology selection using entropy-weighted TOPSIS technique: The case study of Lagos, Nigeria. *Energy*, 201:117675, 2020.

[6] Anvari, S., Taghavifar, H., and Parvishi, A. Thermo-economical consideration of Regenerative organic Rankine cycle coupling with the absorption chiller systems incorporated in the trigeneration system. *Energy Conversion and Management*, 148:317–329, 2017.

[7] Bejan, A., Tsatsaronis, G., and Moran, M. J. *Thermal design and optimization*. John Wiley & Sons, 1995.

[8] Çelikbilek, Y. and Tüysüz, F. An in-depth review of theory of the TOPSIS method: An experimental analysis. *Journal of Management Analytics*, 7(2): 281–300, 2020.

[9] Cengel, Y. A., Boles, M. A., and Kanoğlu, M. *Thermodynamics: An engineering approach*, volume 5. 2011.

[10] Chitsaz, A., Mehr, A., and Mahmoudi, S. Exergoeconomic analysis of a trigeneration system driven by a solid oxide fuel cell. *Energy Conversion and Management*, 106:921–931, 2015.

[11] Corne, D. W., Jerram, N. R., Knowles, J. D., and Oates, M. J. PESA-II: Region-based selection in evolutionary multiobjective optimization. In *Proceedings of the 3rd annual conference on genetic and evolutionary computation*, pages 283–290, 2001.

[12] Dincer, I. and Al-Muslim, H. Thermodynamic analysis of reheat cycle steam power plants. *international Journal of Energy research*, 25(8):727–739, 2001.

[13] Dincer, I., Rosen, M. A., and Ahmadi, P. *Optimization of energy systems*. 2017.

[14] Ding, P., Liu, X., Qi, H., Shen, H., Liu, X., and Farkoush, S. G. Multi-objective optimization of a new cogeneration system driven by gas turbine cycle for power and freshwater production. *Journal of Cleaner Production*, 288:125639, 2021.

[15] Ganapathy, V. *Steam generators and waste heat boilers: for process and plant engineers*. 2014.

[16] Heidarnejad, P., Genceli, H., Asker, M., and Khanmohammadi, S. A comprehensive approach for optimizing a biomass assisted geothermal power plant with freshwater production: Techno-economic and environmental evaluation. *Energy Conversion and Management*, 226:113514, 2020.

[17] Huang, J. Combining entropy weight and TOPSIS method for information system selection. In *2008 ieee conference on cybernetics and intelligent systems*, pages 1281–1284, 2008.

[18] Jingwen Huang. Combining entropy weight and TOPSIS method for information system selection. In *2008 IEEE Conference on Cybernetics and Intelligent Systems*, pages 1281–1284, Chengdu, China, 2008.

[19] Karthikeyan, R., Hussain, M. A., Reddy, B., and Nag, P. Performance simulation of heat recovery steam generators in a cogeneration system. *International Journal of Energy Research*, 22(5):399–410, 1998.

[20] Khaljani, M., Saray, R. K., and Bahlouli, K. Comprehensive analysis of energy, exergy and exergo-economic of cogeneration of heat and power in a combined gas turbine and organic Rankine cycle. *Energy Conversion and Management*, 97:154–165, 2015.

[21] Khaljani, M., Saray, R. K., and Bahlouli, K. Thermodynamic and thermoeconomic optimization of an integrated gas turbine and organic rankine cycle. *Energy*, 93:2136–2145, 2015.

[22] Lemmon E, Huber M, M. M. NIST Standard Reference Database 23, Reference Fluid Thermodynamic and Transport Properties (REFPROP), version 9.0, National Institute of Standards and Technology, R1234yf. fld file dated December 22 (2010). Technical report, NIST. URL `https://www.nist.gov/system/files/documents/srd/REFPROP8_manua3.htm`.

[23] Nag, P. *Power plant engineering*. 2008.

[24] Nazari, N., Heidarnejad, P., and Porkhial, S. Multi-objective optimization of a combined steam-organic Rankine cycle based on exergy and exergo-economic analysis for waste heat recovery application. *Energy conversion and management*, 127:366–379, 2016.

[25] Nondy, J. and Gogoi, T. Exergoeconomic investigation and multi-objective optimization of different ORC configurations for waste heat recovery: A comparative study. *Energy Conversion and Management*, 245:114593, 2021.

[26] Nondy, J. and Gogoi, T. K. Comparative performance analysis of four different combined power and cooling systems integrated with a topping gas turbine plant. *Energy Conversion and Management*, 223:113242, 2020.

[27] Oko, C. and Njoku, I. Performance analysis of an integrated gas-, steam-and organic fluid-cycle thermal power plant. *Energy*, 122:431–443, 2017.

[28] Owebor, K., Oko, C. O. C., Diemuodeke, E., and Ogorure, O. J. Thermo-environmental and economic analysis of an integrated municipal waste-to-energy solid oxide fuel cell, gas-, steam-, organic fluid-and absorption refrigeration cycle thermal power plants. *Applied energy*, 239:1385–1401, 2019.

[29] Safarian, S. and Aramoun, F. Energy and exergy assessments of modified Organic Rankine Cycles (ORCs). *Energy reports*, 1:1–7, 2015.

[30] Salmi, W., Vanttola, J., Elg, M., Kuosa, M., and Lahdelma, R. Using waste heat of ship as energy source for an absorption refrigeration system. *Applied Thermal Engineering*, 115:501–516, 2017.

[31] Sayyaadi, H. Multi-objective approach in thermoenvironomic optimization of a benchmark cogeneration system. *Applied Energy*, 86(6):867–879, 2009.

[32] Shukla, A. K., Sharma, A., Sharma, M., and Nandan, G. Thermodynamic investigation of solar energy-based triple combined power cycle. *Energy Sources,*

Part A: Recovery, Utilization, and Environmental Effects, 41(10):1161–1179, 2019.

[33] Singh, O. K. and Kaushik, S. Variables influencing the exergy based performance of a steam power plant. *International journal of green energy*, 10(3): 257–284, 2013.

[34] Towler, G. and Sinnott, R. *Chemical engineering design: principles, practice and economics of plant and process design*. Butterworth-Heinemann, 2021.

[35] Wang, S., Liu, C., Li, J., Sun, Z., Chen, X., and Wang, X. Exergoeconomic analysis of a novel trigeneration system containing supercritical CO2 Brayton cycle, organic Rankine cycle and absorption refrigeration cycle for gas turbine waste heat recovery. *Energy Conversion and Management*, 221:113064, 2020.

[36] Yazdi, B. A., Yazdi, B. A., Ehyaei, M. A., and Ahmadi, A. Optimization of micro combined heat and power gas turbine by genetic algorithm. *Thermal Science*, 19(1):207–218, 2015.